Journal of Asian Earth Sciences 99 (2015) 57–71

Contents lists available at ScienceDirect

Journal of Asian Earth Sciences

journal homepage: www.elsevier.com/locate/jseaes

Zircon U–Pb ages and Hf–O isotopes, and whole-rock Sr–Nd isotopes of the Bozhushan granite, Yunnan province, SW China: Constraints on petrogenesis and tectonic setting

Xiao-Cui Chen [a,b], Rui-Zhong Hu [a,*], Xian-Wu Bi [a], Hong Zhong [a], Jiang-Bo Lan [a], Cheng-Hai Zhao [a,b], Jing-Jing Zhu [a]

[a] State Key Laboratory of Ore Deposits Geochemistry, Institute of Geochemistry, Chinese Academy of Sciences, Guiyang 550005, China
[b] University of Chinese Academy of Sciences, Beijing 100049, China

ARTICLE INFO

Article history:
Received 4 June 2014
Received in revised form 4 December 2014
Accepted 31 December 2014
Available online 9 January 2015

Keywords:
A-type granite
Zircon U–Pb dating
Zircon Hf–O isotope
Sr–Nd isotope
Lithospheric extension
Western Cathaysia block

ABSTRACT

The Bainiuchang silver-polymetallic ore deposit is a super-large deposit in the western part of the South China tungsten–tin province (or the Nanling tungsten–tin province). The deposit is spatially and temporally associated with the Bozhushan granite pluton. Our new data indicate that the Bozhushan granitoids formed at 86–87 Ma. The granitoids are geochemically consistent with A-type granite. The Bozhushan pluton consists predominantly of biotite granite that is characterized by weakly peraluminous to metaluminous compositions and high alkali contents ($Na_2O + K_2O$ = 7.51–9.06 wt.%). The granitic rocks are enriched in large-ion lithophile elements (LILE) Rb, Th, U, and K, but relatively depleted in Ba and Sr. In addition, they have high Zr + Nb + Ce + Y contents (310–478 ppm) and high 10,000× Ga/Al ratios (2.7–3.1). The temperatures of the parental magmas for the Bozhushan granites are estimated to be 790–842 °C based on the zircon saturation thermometer. Isotopically, the Bozhushan granites are characterized by elevated initial $^{87}Sr/^{86}Sr$ ratios (0.7126–0.7257) and low εNd values (−11.2 to −12.4), and high $\delta^{18}O$ values (7.91–9.58‰) and low ε_{Hf} values (−9.5 to −6.1) for zircon crystals, which indicate a dominant continental crustal source. The two-stage Hf model ages vary from 1.53 to 1.86 Ga. The isotopic compositions support the interpretation that the granitic rocks formed by melting of the Meso- and Neoproterozoic metasedimentary basements of the Cathaysia block. These results, together with geological records in the other parts of the western Cathaysia block, suggest that the formation of the Bozhushan A-type granites is related to lithospheric extension and asthenospheric upwelling that are associated with the change of plate motion in Late-Cretaceous.

1. Introduction

South China is well-known for large-scale magmatism and mineralization in the Mesozoic. More than 50% of the world's tungsten and antimony resources, and 20% of the world's tin resources are present in South China. The South China block consists of the Yangtze craton in the north and the Cathaysia block in the south (Fig. 1A). The Nanling tungsten–tin province, which contains hundreds of W–Sn deposits associated with granitic plutons with ages varying from Jurassic to Late Cretaceous, occurs within the Cathaysia block (Hua et al., 2007; Mao et al., 2013, 2007; Pei et al., 2009; Sun et al., 2012) (Fig. 1A). The important tin-polymetallic deposits associated with Cretaceous granitoids are widespread in the western part of the Cathaysia block (Cheng and Mao, 2010; Gu et al., 2009; Liu et al., 2007b; Luo, 1995). The tin-mineralization and associated magmatism are believed to have formed in the geodynamic environment of lithospheric extension and thinning (Cheng et al., 2013b; Feng et al., 2013; Liu et al., 2007b; Yan et al., 2005).

The Bainiuchang silver-polymetallic ore deposit is located in the western part of the Nanling tungsten–tin province, southeastern Yunnan. The genesis of the Bainiuchang deposit has been debated. Some researchers believe that this deposit is a SEDEX-type deposit (Chen et al., 1998; Zhou et al., 1998). Other researchers argue that it is not a typical SEFDEX-type deposit but is significantly modified by the Yanshanian granitic magmatism (Chen et al., 2000; Deng et al., 2004; Zhu et al., 2010). The role of the granite magmatism

* Corresponding author at: Institute of Geochemistry, Chinese Academy of Sciences, 46 Guanshui Road, Guiyang 550002, China. Tel.: +86 851 5891962; fax: +86 851 5891664.
E-mail addresses: cxchyh@163.com (X.-C. Chen), huruizhong@vip.gyig.ac.cn (R.-Z. Hu).

http://dx.doi.org/10.1016/j.jseaes.2014.12.012
1367-9120/

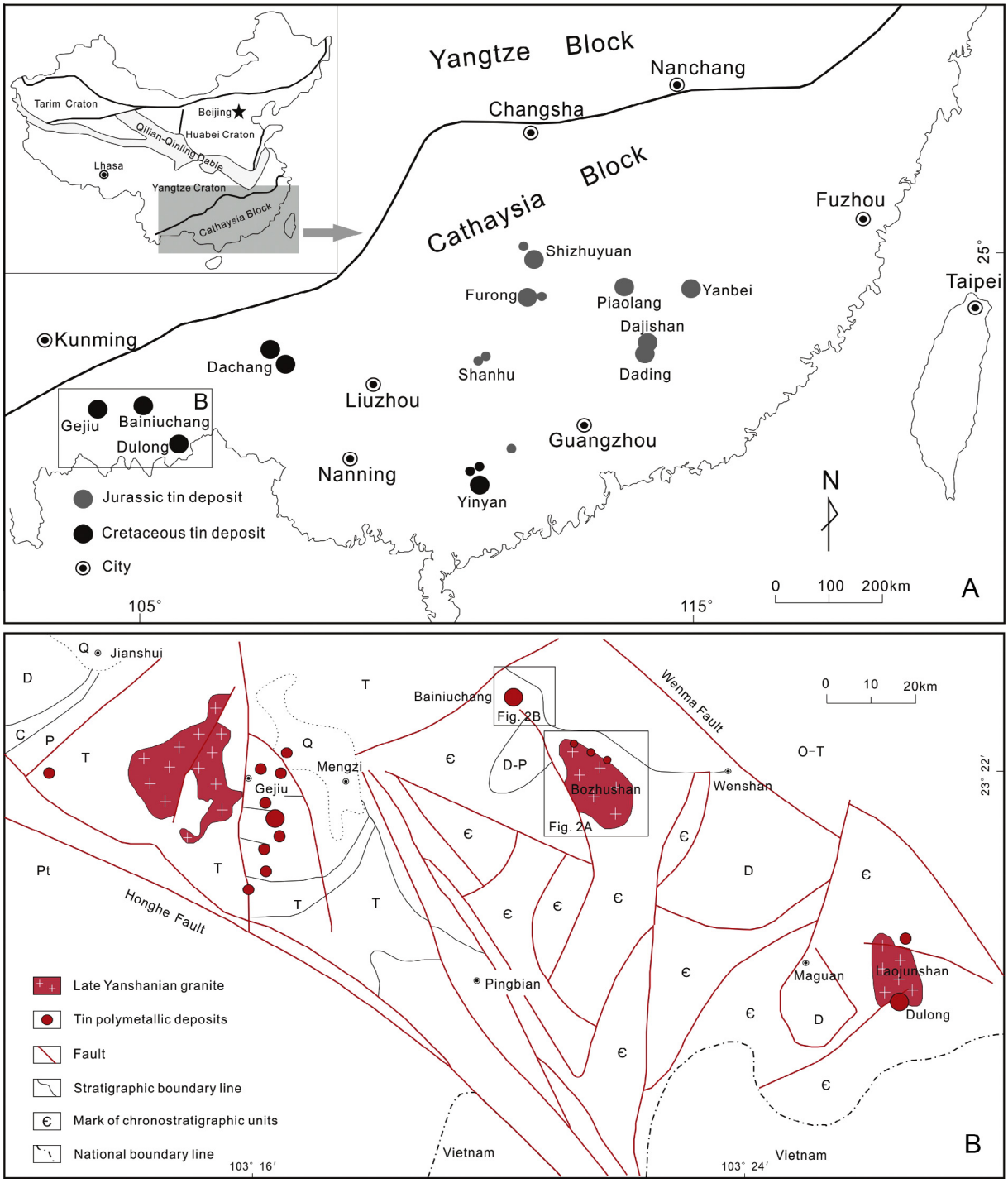

Fig. 1. (A) Distribution of tin deposits in the Cathaysia block (Mao et al., 2007) and (B) sketch showing the distribution of magmatic rocks and tin-polymetallic deposits in southeastern Yunnan province (Zhang et al., 2006).

in the formation of the deposit has been investigated by many researchers recently (Li et al., 2011; Liu et al., 2007a; Zhang et al., 2006, 2011). Spatially, the Bainiuchang deposit and the Bozhushan granite are closely related. Direct LA-MC-ICP-MS U–Pb dating of cassiterite (Li et al., 2013) has established a temporal link between the deposit and the granite pluton. The genetic relationship between the deposit and the pluton is still not clear. Thus, a systematic study of the granite pluton is important.

Previous studies obtained the whole-rock Rb–Sr isochron ages ranging from 96 to 116 Ma (Zhang and Chen, 1997), and zircon U–Pb ages of 85–88 Ma for the Bozhushan granite pluton (Cheng et al., 2010). More precise ages are required to resolve these discrepancies. Moreover, owing to the lack of isotopic data and systematic geochemical data, the petrogenesis and tectonic setting of the granitoids are poorly understood. In this paper, we report major and trace element compositions and Sr–Nd isotopes for whole rock samples and U–Pb ages and Hf–O isotopes for zircon crystals from the Bozhushan granite pluton. We use these data to constrain the petrogenesis and tectonic setting of the pluton.

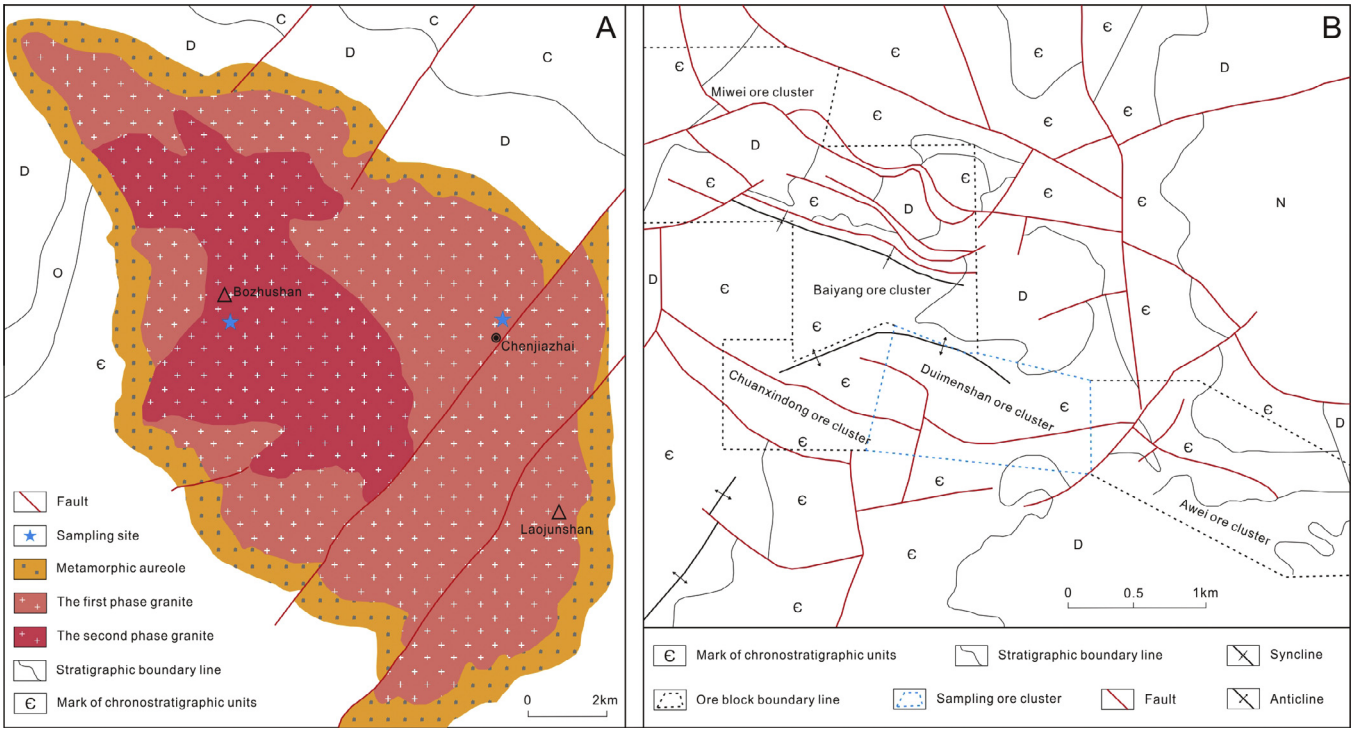

Fig. 2. Simplified geological maps of (A) Bozhushan granitic intrusion (Zhang and Chen, 1997) and (B) Bainiuchang tin-polymetallic deposit.

2. Tectonic and geological background

The South China Block formed by the amalgamation of the Yangtze Craton and the Cathaysia Block in the Early Neoproterozoic. Many researchers believed that the Yangtze Craton and the Cathaysia Block initially collided in the Early Neoproterozoic, separated from each other in the Late Neoproterozoic, and merged again in the Caledonian (Li et al., 2009a, 2003, 2010; Yan et al., 2005).

The Bainiuchang tin-polymetallic deposit is a member of the southeast Yunnan tin-polymetallic metallogenic belt in the western part of the Cathaysia block (Fig. 1A). This deposit is located in the southeastern part of Yunnan province. Three granitic intrusions, named Gejiu, Bozhushan, and Laojunshan, host three super-large tin-polymetallic deposits (i.e., Gejiu, Bainiuchang, and Dulong, respectively), which form equidistant outcrops in the southeast Yunnan tin-polymetallic metallogenic belt (Fig. 1B). These intrusions and tin-mineralization events are considered to have formed in a lithospheric extension and thinning setting during the Late Cretaceous (Cheng et al., 2013a; Liu et al., 2007b; Zhang et al., 2006, 2011).

The Bainiuchang–Bozhushan area is an important tin-polymetallic ore district in the southeastern Yunnan tin-polymetallic metallogenic belt. Granites and spatially related tin mineralizations are extensively developed in the Bainiuchang–Bozhushan area (Fig. 1B). The major sedimentary strata in this area are the Cambrian (Є), Ordovician (O), Devonian (D), Carbonic (C), Permian (P), and Triassic (T) carbonate rocks. The most prominent structures are the NE-trending regional tectonic terranes, the NE- to EW-trending regional faults and the NWW- to NS-trending local faults. These structures appear to have controlled the distribution of granitic intrusions and associated ore deposits (Fig. 2A and B). The Bainiuchang silver-polymetallic ore deposit was discovered in the 1980s. It contains Ag (6470 t), Zn (172 Mt), Pb (110 Mt), and Sn (7 Mt) (Luo, 1995). The deposit consists of five clusters of ore bodies, namely the Baiyang, Duimenshan, Miwei, Chuanxindong and Awei that are distributed along the same structural lineament as the Bozhushan granite. Recent drilling has intercepted granite at depths from 1250 to 1420 m in the southern part and the northern part of the ore deposit (Liu et al., 2007a). Numerous granitic porphyry bodies and monzonite veins have been found at depth in the Chuanxindong and Duimenshan ore clusters. The Bozhushan granite, which is located 7 km southeast of the Bainiuchang deposit, may be connected to the concealed granite bodies (Zhang et al., 2006, 2009). Systematic studies of the Bozhushan granite will significantly promote an understanding of the genesis of the Bainiuchang silver-polymetallic ore deposit. Furthermore, the granitic porphyry occured at depth in ore clusters is also prepared for our study, for this could offer a better genetic link between the ore deposit and the granite.

3. Granite petrography and sample description

The surface exposure of the Bozhushan granitic pluton has a fusiform shape with NW-trending. It is approximately 18 km long and 10 km wide, with a total surface exposure of ca. 120 km^2. The granite pluton intruded the Cambrian (Є) to Devonian (D) carbonate and clastic rocks. Contact metamorphism is present in many places (Fig. 2A). It was previously divided into two intrusive phases: an Early Cretaceous intrusive phase and a later Late Cretaceous intrusive phase (Fig. 2A) (Zhang and Chen, 1997). A total of 10 samples were collected from the Bozhushan granitic pluton. Samples BZS-1 and BZS-5, which are collected from the two intrusive phases respectively, were used for zircon U–Pb dating. The major rock types of the Bozhushan granitic pluton are medium- to coarse-grained biotite granites. Its main minerals are K-feldspar (25–35 vol.%), plagioclase (22–30 vol.%), quartz (25–31 vol.%) and biotite (6–10 vol.%). Twin texture of plagioclase is common in the samples (Fig. 3, samples BZS-1 and BZS-5). The main ferromagnesian mineral is biotite. Accessory minerals include apatite, allanite, zircon and ilmenite.

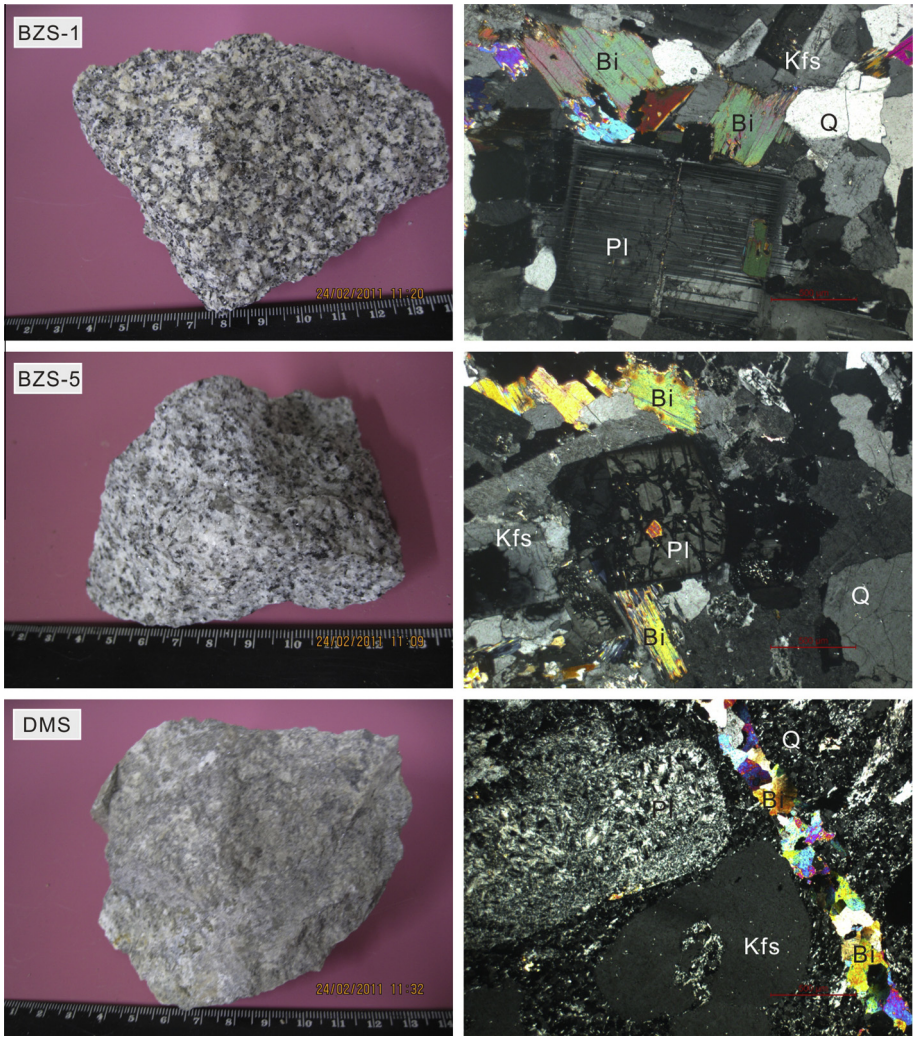

Fig. 3. Photographs and photomicrographs of granitic samples from the Bozhushan granitic intrusion (samples BZS-1 and BZS-5) and granite porphyry veins occurring in the Duimenshan ore block of the Bainiuchang ore district (DMS). BZS-1 and BZS-5 are coarse-grained granites; DMS is fine-grained granite porphyry.

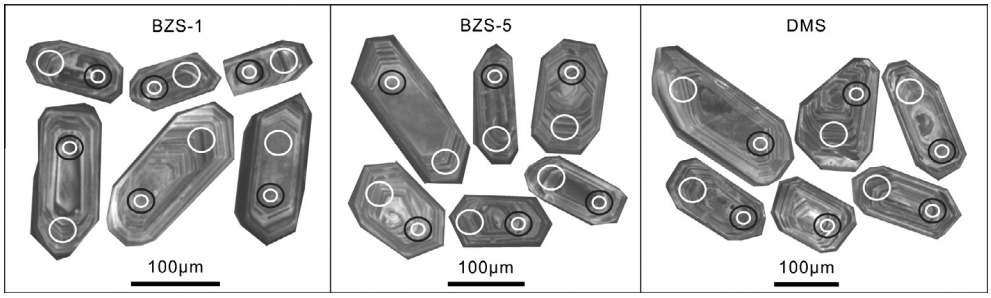

Fig. 4. Cathodoluminescence (CL) images of zircon grains (BZS-1 and BZS-5 obtained from the Bozhushan granitic intrusion; DMS from the Duimenshan ore block of the Bainiuchang ore district). Large white ellipses delineate the LA-MC-ICP-MS analyzing spots for U–Pb dating; small white circles denote the analyzing spots for O isotopes; black circles mark the analyzing spots for Hf isotopes.

The sample with an abbreviation of DMS was collected from small granitic porphyry dykes underground in the Duimenshan ore cluster of the Bainiuchang ore deposit. The granitic porphyry sample contains fine-grained K-feldspar (38 vol.%), plagioclase (32 vol.%), quartz (20–30 vol.%) and biotite (5 vol.%). The texture of this sample is illustrated in Fig. 3. This sample was also used for zircon U–Pb dating as well as chemical analysis.

4. Analytical methods

Zircon grains in the samples from the Bozhushan granite pluton (sample BZS-1 and BZS-5) and the associated granitic porphyry dyke (sample DMS) in the Bainiuchang ore district were separated using conventional technique including heavy liquid and magnetic separation. Transparent and euhedral zircon crystals were selected

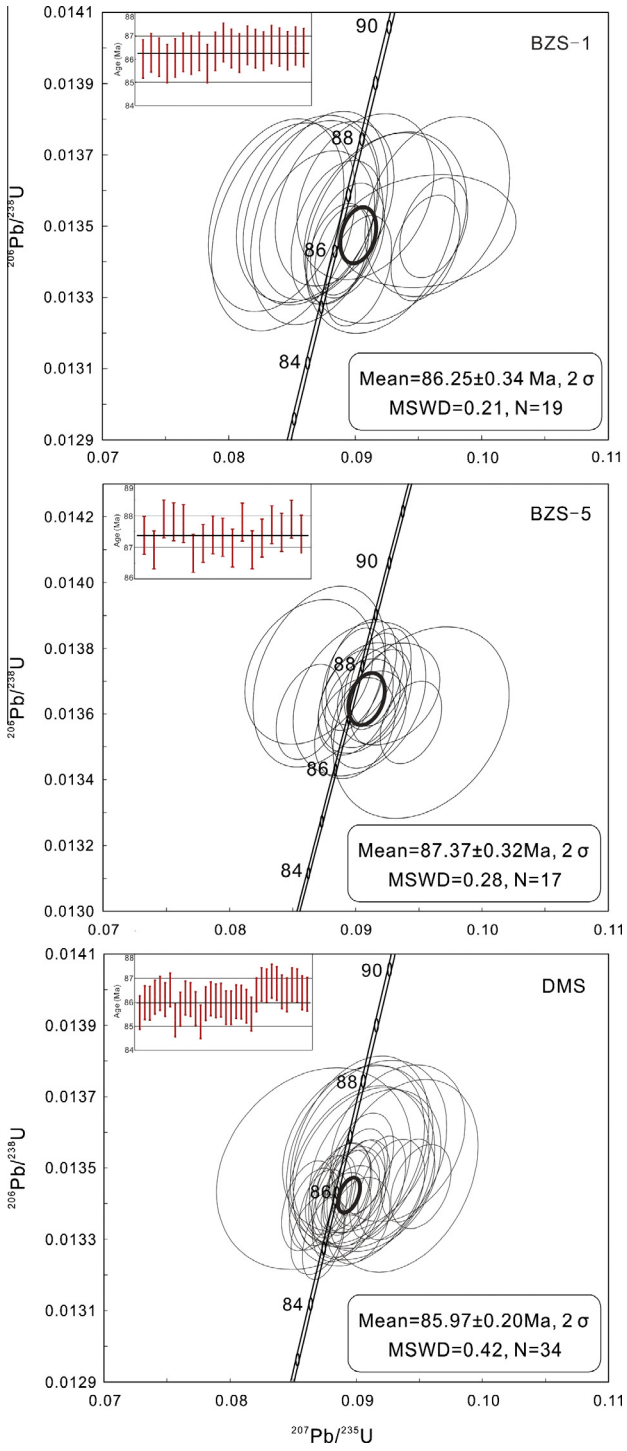

Fig. 5. U–Pb concordia diagram and weighted average $^{206}Pb/^{238}U$ ages of zircons from the three samples (BZS-1, BZS-5, and DMS).

under a binocular microscope. The selected zircon crystals were mounted on an epoxy resin disk, polished and then coated with gold. The textures and morphologies of the zircon grains were documented using optical microphotographs and cathodoluminescence (CL) images. The CL images were obtained using a LEO1450VP scanning electron microscope at the Institute of Geology and Geophysics, Chinese Academy of Sciences (IGGCAS), Beijing. The U–Pb isotopic analyses were performed at the State Key Laboratory of Geological Processes and Mineral Resources, China University of Geosciences. Laser sampling was performed on a GeoLas 2005 System. The ion signal intensities of samples were acquired using an Agilent 7500a ICP-MS instrument. The 91500 zircon standard was used as standard. Helium and argon were used as carrier and make-up gas, respectively. The gas flows were optimized using the NIST SRM 610 standard to obtain maximum signal intensity. The analytical procedures were the same as those used for zircon U–Pb dating in the same laboratory (Liu et al., 2010b).

Zircon oxygen isotopes were measured using the Cameca IMS-1280 SIMS at the IGGCAS. The analytical procedures were described in detail by Li et al. (2009b). Following U–Pb analysis, the sample mount was re-ground to ca. 5 μm to ensure that any oxygen implanted on the zircon surface was completely removed. The ion source was a Cs^+ primary ion beam. Oxygen isotopes were measured in multi-collector mode using two off-axis Faraday cups. The laser was focused to produce an ablation pit with an approximate diameter of 20 μm, with one analysis taking ca. 3 min. The instrumental mass fractionation factor was corrected using the zircon 91500 standard which has a $\delta^{18}O$ value of 9.9‰.The measured $^{18}O/^{16}O$ ratios were normalized to the value of Vienna Standard Mean Ocean Water (VSMOW, $^{18}O/^{16}O = 0.0020052$) (Li et al., 2009b).

Lu–Hf isotopic analysis was performed on a Nu plasma multi-collector ICP-MS equipped with a UP-213 laser ablation system (LA-MC-ICP-MS) at the IGGCAS. The Lu–Hf isotopic measurements were performed on the zircon grains that were previously analyzed for U–Pb and O isotopes. The diameters of the ablation pits are 40–80 μm. The laser beam had an energy density of 10 J/cm^2, a repetition rate of 8–10 Hz and ablation time of 26 s. The analytical procedures were similar to those given in Wu et al. (2006).

Major elements in whole rocks were analyzed using the Axios PW4400 X-ray fluorescence spectrometer (XRF) at the State Key Laboratory of Ore Deposit Geochemistry (SKLODG), Institute of Geochemistry, Chinese Academy of Sciences, in Guiyang, On fused lithium-tetraborate glass pellets. The analytical precision was better than 5%. Trace elements in whole rocks were analyzed using a PE DRC-e ICP-MS at the SKLODG. About 50 mg of sample powder was dissolved in high-pressure Teflon bombs. Rh was used as an internal standard to monitor signal drift during analysis. The analytical procedures were similar to those given in Qi et al. (2000).

Whole-rock Sr–Nd isotopes were analyzed using a Triton thermal ionization mass spectrometer at the SKLODG. The samples were first dissolved in the mixture of HF, HNO_3, and $HClO_4$ in Teflon bombs. Sr, Rb, Sm and Nd were then separated by cation-exchange in the HDEHP-coated Kef columns. The mass fractionation corrections for Sr and Nd isotopic ratios were based on $^{86}Sr/^{88}Sr = 0.1194$ and $^{146}Nd/^{144}Nd = 0.7219$, respectively. The $^{87}Sr/^{86}Sr$ ratio of the NBS987 Sr standard was determined to be 0.710258 ± 7 ($2\sigma_m$). The $^{143}Nd/^{144}Nd$ ratios of the La Jolla and JNDI-1 Nd standard solutions were determined to be 0.511841 ± 3 ($2\sigma_m$) and 0.512104 ± 5 ($2\sigma_m$), respectively.

5. Results

5.1. Zircon U–Pb ages

Zircon grains from three samples (BZS-1, BZS-5, and DMS) were selected for U–Pb dating by LA-ICP-MS. The selected zircon crystals are light pink to colorless and transparent. They are mostly euhedral and 100–300 μm in length, with length-to-width ratios varying from 2:1 to 3:1. The CL images of the selected grains commonly show concentric oscillatory zoning (Fig. 4). These features are common for magmatic zircon crystals. No inherited zircon grains were found in the samples. The average age of zircon crystals from each sample was calculated based on the error-weighted mean of the common Pb-corrected $^{206}Pb/^{238}U$ ages at

Table 1
Major element (in%), trace element (in ppm) contents of the Bozhushan granitic intrusion (BZS) and granite-porphyry veins in Bainiuchang ore district (DMS).

Sample no.	DMS	BZS-1	BZS-2	BZS-3	BZS-4	BZS-5	BZS-6	BZS-7	BZS-8	BZS-9	BZS-10
SiO_2	64.27	68.22	67.43	69.25	67.86	66.05	65.81	71.04	67.33	67.10	66.77
Al_2O_3	14.70	14.99	14.66	15.08	15.10	14.27	14.41	14.65	14.29	14.53	14.72
Fe_2O_3	3.16	3.65	3.44	3.46	3.49	2.98	3.30	2.41	3.73	3.62	3.97
MgO	1.19	1.33	1.28	1.28	1.29	1.05	1.35	0.95	1.25	0.86	0.93
CaO	2.70	2.36	2.34	2.35	2.36	2.09	2.67	2.33	3.25	2.08	2.23
Na_2O	3.14	2.88	3.40	3.26	3.32	3.13	3.70	3.92	3.50	3.38	3.40
K_2O	4.54	4.64	4.60	4.53	4.79	5.16	5.00	5.14	4.63	4.66	4.99
TiO_2	0.67	0.63	0.60	0.60	0.60	0.65	0.56	0.40	0.60	0.56	0.56
MnO	0.16	0.06	0.06	0.06	0.06	0.04	0.04	0.04	0.06	0.06	0.05
P_2O_5	0.30	0.27	0.26	0.26	0.27	0.23	0.24	0.25	0.27	0.27	0.24
LOI	9.53	0.69	0.94	1.07	1.23	1.01	4.36	1.26	1.03	1.37	1.64
Rb	373	291	290	276	271	309	288	313	278	365	309
Sr	332	376	368	361	377	343	360	301	359	361	379
Ba	868	988	925	872	992	970	953	875	879	896	909
Th	30.3	40.2	34.2	41.5	45.5	41.5	28.1	43.1	42.4	35.8	38.7
U	8.8	10.4	14.0	8.5	11.3	10.3	14.6	8.3	15.1	12.6	11.6
Nb	30.2	36.1	34.1	35.4	34.1	37.0	33.9	27.0	30.5	24.0	28.5
Ta	2.0	2.6	2.5	3.4	2.4	2.7	2.6	3.6	2.9	2.7	2.4
Zr	264.0	235.0	230.0	157.0	225.0	227.1	221.0	146.0	182.0	187.0	198.0
Hf	6.9	6.2	6.3	4.2	6.2	6.7	6.0	4.0	5.4	5.2	5.1
Sn	134.2	8.6	5.8	8.4	6.7	10.9	13.0	9.5	3.9	4.2	4.7
Ag	4.8	0.3	0.3	0.3	0.3	0.5	0.4	0.3	0.4	0.3	0.3
Zn	955.0	76.2	63.7	60.3	59.9	20.8	43.8	38.8	57.6	61.0	54.1
Cu	396.0	6.9	6.4	4.8	8.1	8.2	66.4	14.1	6.5	8.2	7.1
La	78.8	81.2	87.6	72.3	77.6	83.1	85.2	54.4	71.6	69.4	69.7
Ce	140.0	142.0	155.0	130.0	137.0	96.0	146.0	98.8	138.0	134.0	134.0
Pr	15.6	15.6	16.8	14.6	15.1	10.8	16.3	10.6	15.5	15.3	15.4
Nd	54.2	52.7	57.3	50.8	52.8	53.1	55.7	35.8	56.1	53.9	52.1
Sm	8.8	8.3	9.5	8.9	8.6	8.9	9.2	6.3	8.7	9.1	8.8
Eu	1.4	1.4	1.5	1.3	1.5	1.1	1.4	1.0	1.5	1.6	1.4
Gd	6.3	5.7	6.5	6.0	5.8	6.9	6.4	5.9	5.7	6.0	5.8
Tb	1.0	0.9	1.0	0.9	0.9	0.8	0.9	0.7	0.9	0.9	0.9
Dy	4.7	3.9	4.5	4.6	4.3	4.4	4.1	3.4	3.9	4.5	3.9
Ho	1.0	0.8	0.9	0.9	0.9	0.8	0.8	0.6	0.9	0.8	0.9
Er	2.6	2.2	2.5	2.4	2.4	2.0	2.2	1.7	2.7	2.5	2.6
Tm	0.4	0.3	0.3	0.3	0.3	0.3	0.3	0.2	0.3	0.3	0.3
Yb	2.3	2.1	2.3	2.2	2.2	1.8	2.1	1.5	1.9	2.3	1.8
Lu	0.3	0.3	0.3	0.3	0.3	0.3	0.3	0.2	0.3	0.4	0.3
Y	44.0	51.6	52.6	49.5	49.5	68.4	46.7	38.3	44.9	38.9	41.9
Rb/Sr	1.1	0.8	0.8	0.8	0.7	0.9	0.8	1.0	0.8	1.0	0.8
10,000 Ga/Al	2.97	3.03	3.03	2.76	2.93	3.14	2.81	2.66	2.80	2.90	2.90
T/°C	842.31	853.41	846.72	853.86	850.26	847.24	832.26	846.89	826.29	853.01	849.06

95% confidence level. These ages are interpreted to represent the emplacement ages of the granites.

The results of zircon U–Pb dating for all of the samples are given in Appendix Table A1. The uranium and thorium contents in the zircons vary significantly (U, 655–2745 ppm; Th, 265–1345 ppm). The Th/U ratios range from 0.19 to 0.77. The $^{206}Pb/^{238}U$ ages of 19 zircon grains from sample BZS-1 are 85.7–87.0 Ma, with a weighted average age of 86.3 ± 0.3 Ma (MSWD = 0.21; 2σ) (Fig. 5, BZS-1). The $^{206}Pb/^{238}U$ ages of 17 zircon grains from sample BZS-5 are between 86.8 and 87.9 Ma, with a weighted average of 87.4 ± 0.3 Ma (MSWD = 0.28; 2σ) (Fig. 5, BZS-5). The $^{206}Pb/^{238}U$ ages of 34 zircon grains from the DMS sample are between 85.2 and 86.9 Ma, with a weighted average of 86.0 ± 0.2 Ma (MSWD = 0.42; 2σ) (Fig. 5, DMS). The results show that the granite porphyry dyke (the DMS sample) and the second intrusive phase of the Bozhushan pluton in the Bainiuchang ore district have the same age within the analytical error. The first intrusive phase of the Bozhushan pluton (sample BZS-5) is slightly older by ~1 Ma. All of these three intrusive phases were emplaced in the Late Cretaceous.

5.2. Major and trace element compositions

The major and trace element compositions of 11 samples from the Bozhushan pluton and the associated granite porphyry dyke in the Bainiuchang ore district are listed in Table 1. The SiO_2 contents range from 64.27 wt.% (DMS) to 71.04 wt.% (BZS-7). In the whole-rock SiO_2 vs. ($K_2O + Na_2O$) classification diagram (Fig. 6A), most of the samples plot in the alkali field due to relatively high $K_2O + Na_2O$ contents. In the K_2O vs. SiO_2 diagram (Fig. 6B), all of the samples plot in the high-K and shoshonitic fields. The Al_2O_3 contents of the samples range from 14.3 to 15.1 wt.%. Based on the plot of A/NK (molar ratio of $Al_2O_3/[Na_2O + K_2O]$) vs. A/CNK (molar ratio of $Al_2O_3/[CaO + K_2O + Na_2O]$), most of the samples are classified as metaluminous to weakly peraluminous granites (Fig. 6C).

All of the samples have element compositions similar to those of A-type granites. They have high abundances of high field strength elements such as Zr (146–264 ppm) and Y (38.3–68.4 ppm). The total amounts of Zr + Nb + Ce + Y in the samples are 310–478 ppm. The 10,000× Ga/Al ratios of the samples are 2.7–3.1, with an average of 2.9. This value is slightly higher than the global average of 2.6 for A-type granite (Whalen et al., 1987). In the primitive mantle-normalized diagram (Fig. 7A), all of the samples show negative Ba, Sr, Nb, and Ti anomalies and positive Rb, Th, U, K and Nd anomalies. In the chondrite-normalized diagram, all of the samples show light REE enrichments relative to heavy REE ($(La/Yb)_N$ = 31–46) and negative Eu anomalies (Fig. 7B).

The zircon saturation temperatures (T, °C), calculated from bulk rock compositions using the equation of Watson and Harrison (1983), may represent the minimum temperature of the parental magma. The results of our calculations are listed in Table 1. The

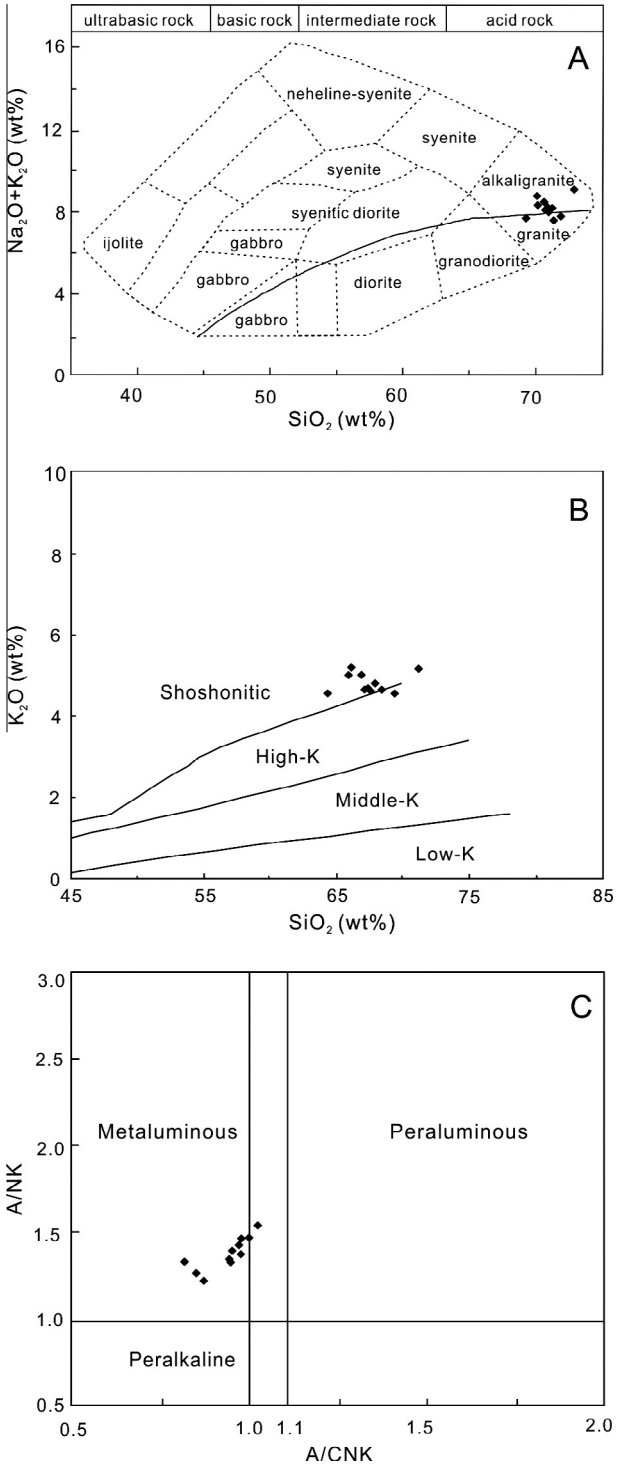

Fig. 6. Classification diagrams of Bozhushan granitic intrusion and granite porphyry veins in the Bainiuchang ore district: (A) SiO_2 vs. ($K_2O + K_2O$), (B) SiO_2 vs. K_2O, and (C) A/NK (molar ratio of $Al_2O_3/[Na_2O + K_2O]$) vs. A/CNK (molar ratio of $Al_2O_3/[CaO + K_2O + Na_2O]$). Fields in diagrams (A) and (B) after Middlemost (1994) and Rickwood (1989), respectively.

calculated zircon saturation temperatures are 790–842 °C, with an average of 819 °C (Fig. 8).

5.3. Zircon Hf–O isotopes

A total of 57 zircon grains from three samples (BZS-1, BZS-5, and DMS) were analyzed for Hf and O isotopic compositions. Among them 55 grains were measured for U–Pb ages. The Hf and O isotopic data are given in Appendix Table A2. The $\varepsilon_{Hf}(t)$ values and two-stage model ages were calculated using the average zircon U–Pb ages of the samples. The Hf and O isotopic compositions of the zircon grains are $^{176}Hf/^{177}Hf = 0.282450–0.282548$, $\varepsilon_{Hf}(t) = -9.5$ to -6.1 and $\delta^{18}O = 7.9–9.6‰$, with the average values of $\varepsilon_{Hf}(t) = -7.7$ and $\delta^{18}O = 8.7‰$ (Fig. 9). The calculated two-stage model ages for the zircon grains are 1534–1749 Ma.

5.4. Sr–Nd isotopes

The whole-rock Sr and Nd isotopic data are given in Table 2. The initial $^{87}Sr/^{86}Sr$ ratios and $\varepsilon_{Nd}(t)$ values, calculated using the average zircon U–Pb ages of the samples, are from 0.7126 to 0.7251 and from −11.2 to −12.0, respectively. This observation, together with the two-stage model ages of 1802 to 1866 Ma for the zircon grains, indicates a Proterozoic crustal source for the granites.

6. Discussion

6.1. A-type granite affinity for the Bozhushan pluton

A-type granite was first used to describe a group of granitic rocks with high alkaline contents and anhydrous compositions in an anorogenic setting (Loiselle and Wones, 1979). Although there is still much debate on the origin of A-type granite, its unique mineralogical and geochemical characteristics are widely recognized. A-type granitoids have high K_2O, Fe/Mg, and incompatible elements such as REE (except Eu), Zr and Hf, but low Al_2O_3, CaO, Ba, Sr and Eu contents (Collins et al., 1982). They are characterized by alkali contents ($K_2O + Na_2O > 8.0$ wt.%), abundant field strength elements (Zr + Nb + Ce + Y > 350 ppm) and high Ga/Al ratios (10,000× Ga/Al > 2.6) (Whalen et al., 1987). A-type granitoids belong to the alkaline and peralkaline series, containing abundant Fe–Mg silicate minerals such as Fe-rich biotite and amphibole (Bonin, 2007). In contrast, S-type granitoids commonly belong to the calc-alkaline series with ASI > 1.1, containing abundant Al-rich silicate minerals such as muscovite, garnet, and cordierite (Chappell and Wyborn, 2012; Clemens, 2003; Ishihara, 2007). A-type granitoids are commonly more enriched in alkaline and HFSE elements (Zr, Nb, Y, REE, and Ga) than I-type granitoids. Many researchers believe that A-type granitoids formed by anhydrous and high-temperature felsic magmas (Clemens et al., 1986; Patiño Douce, 1997).

The mineralogical and geochemical characteristics of the Bozhushan biotite-bearing granitoids are similar to those of A-type granite. As shown in Fig. 6C, the A/CNK values of the Bozhushan metaluminous granitoids are <1.1. The Bozhushan samples are also characterized by relatively high alkali contents and high large-ion lithophile elements (LILE) abundance including Rb, Th and U, and depletion in Ba and Sr. In addition, they have comparatively high Zr + Nb + Ce + Y contents (310–478 ppm), 10,000× Ga/Al ratios (averaging 2.9), and zircon saturation temperatures (790–842 °C). In granite discrimination diagrams (Fig. 10), all samples are plotted in the A-type granite field. These geochemical signatures are clearly characteristic of A-type granites.

6.2. Petrogenesis

A-type granitoids are widely distributed in time and space globally, indicating diverse sources and various formation processes. The major debates include the depths of the crustal sources and the role of the mantle in terms of source and heat. Several genetic models have been proposed for A-type granitoids: (1) partial melting of the residual granulites in the lower crust after melt extrac-

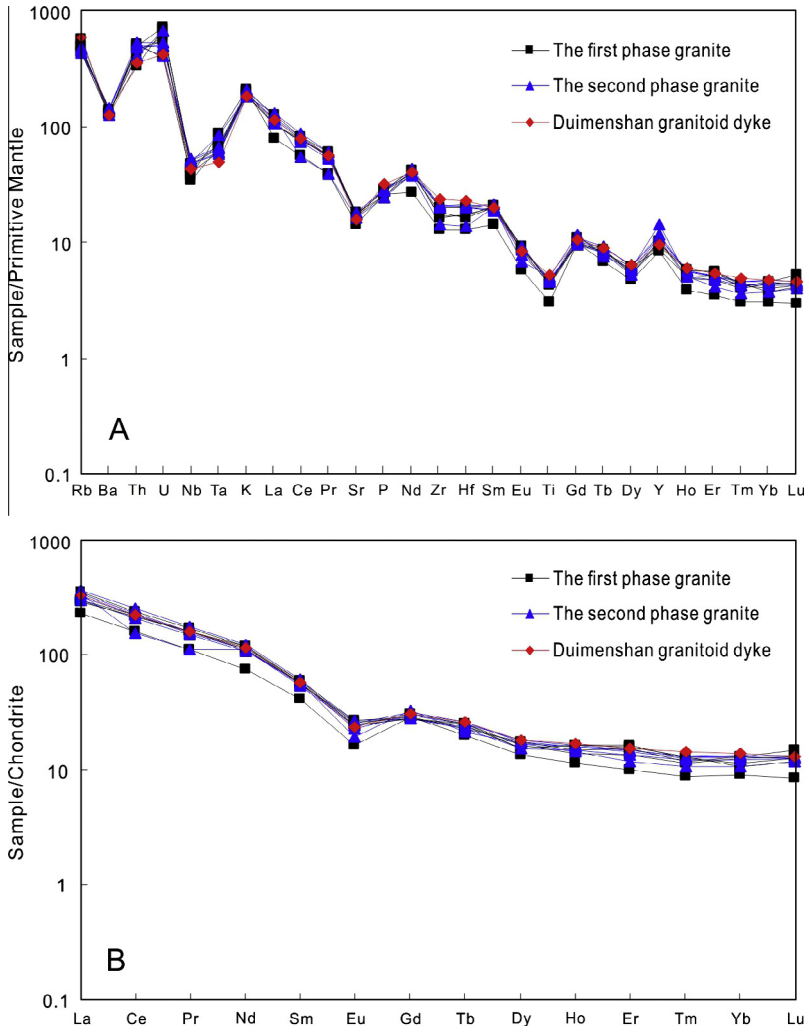

Fig. 7. Primitive mantle-normalized trace element concentrations (A) and chondrite-normalized rare earth element distribution patterns (B) of Bozhushan granitic intrusion and granite porphyry veins in the Bainiuchang ore district. Primitive mantle-normalized values and chondrite-normalized values are from Sun and McDonough (1989).

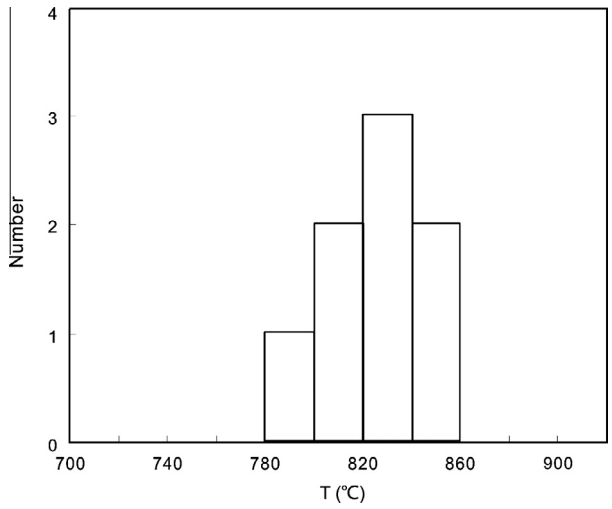

Fig. 8. Histogram of saturation temperatures of zircon from the Bozhushan granitic intrusion and granite porphyry veins in the Bainiuchang ore district.

tion to form I-type granite previously (Collins et al., 1982; King et al., 1997; Whalen et al., 1987); (2) partial melting of a newly-formed crust by underplating of mantle-derived basaltic magmas (Frost and Frost, 1997; Haapala et al., 2005; Wang et al., 2010; Wu et al., 2002); (3) fractionation of mantle-derived mafic magmas (Eby, 1990; Litvinovsky et al., 2002; Turner et al., 1992); (4) hybridization of mantle-derived mafic magma and crust-derived granitic melt (Kerr and Fryer, 1993; Yang et al., 2006; Zhao et al., 2012); (5) low-pressure melting of calc-alkaline rocks at the upper crustal levels (Anderson, 1983; Patiño Douce, 1997; Skjerlie and Johnston, 1993).

To evaluate the competing models, it is important to identify different components in the parental magmas. Incompatible trace element ratios and Sr–Nd–Pb isotopes are useful for this purpose. However, the interpretations of these data are not always simple, especially for granitoids with high Rb/Sr ratios due to high degree of fractionation (Chappell et al., 1987; Chappell and White, 1992; Kemp et al., 2007; Wu et al., 2002). The oxygen isotopes of zircon crystals are more effective in identifying the contributions from the mantle to the parental magmas of granites (Kemp et al., 2007; King et al., 1998; Li et al., 2009b; Valley et al., 1994) because mantle-derived magma ($\delta^{18}O$ value = 5.3 ± 0.3‰; King et al., 1998; Valley et al., 1998) and crust-derived magma ($\delta^{18}O$ value = 10–30‰; Valley et al., 2005) have significantly different O isotopic

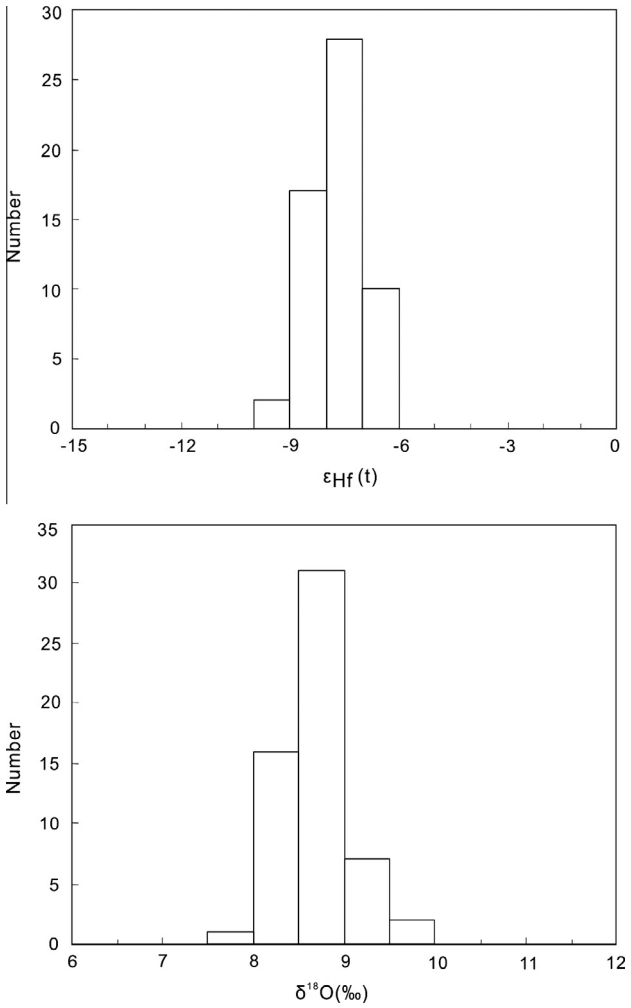

Fig. 9. Histogram of $\varepsilon_{Hf}(t)$ and $\delta^{18}O$ values for the zircons from the Bozhushan granitic intrusion and granite porphyry veins in the Bainiuchang ore district.

compositions. In addition, magmatic zircons have high Hf concentrations (commonly as high as 1 wt.%) and low Lu/Hf ratios (mostly < 0.01), and their Hf isotopic compositions are not susceptible to hydrothermal alteration (Goodge and Vervoort, 2006). As a result, the Hf isotopic compositions of zircon crystals can also be used to evaluate the sources of the parental magmas for granites (Li et al., 2009b; Wu et al., 2007). Therefore, the combination of whole-rock trace element ratios and Sr–Nd–Pb isotopic compositions plus zircon Hf–O isotopes is most effective in deciphering the involvement of mantle-derived magma in the genesis of granites.

As shown in Fig. 7, the Bozhushan granitoids exhibit negative anomalies of HFSEs (Nb, Ta and Ti), possibly due to fractionation of Ti-bearing phases such as ilmenite and titanite. The samples also show slightly negative Eu and Sr anomalies, possibly due to fractionation of plagioclase. The depletion of Ba in the samples could be due to fractionation of K-feldspar and/or plagioclase. The negative anomalies of HFSEs (Nb, Ta and Ti) coupled with positive anomalies of LILEs in the primitive mantle-normalized patterns of these samples are consistent with their derivation from a continental crustal source (Rudnick and Fountain, 1995). These granites have extremely high and variable $(^{87}Sr/^{86}Sr)_I$ ratios (0.71257–0.72505). Their I_{Sr} values with very large uncertainties due to high Rb/Sr ratios indicate their initial $^{87}Sr/^{86}$29 Sr ratios should not be used for the discussion on their source rocks (Jahn et al., 2000; King et al., 1997; Wu et al., 2000). However, all of the samples have fairly constant Nd isotopic compositions and low $\varepsilon_{Nd}(t)$ values (−11.4 to −12.4) plus the two-stage model ages of 1802–1866 Ma, which support the interpretation that they formed by partial melting of the Proterozoic metasedimentary basement in the Cathaysia block (Shen et al., 1995) (Fig. 11A).

As mentioned above, A-type granites commonly formed by low f_{H2O} and high temperature magma derived from a crustal source that was dehydrated and melted previously. Granulitic metavolcanic rocks or metasedimentary rocks are the common rock types in this type of crustal source (Collins et al., 1982). However, such a crustal source cannot produce magmas with high alkaline contents coupled with intermediate SiO_2 concentration such as those of the Bozhushan granitoids (see Clemens, 2006). The high zircon saturation temperatures of the parental magmas for the Bozhushan granitoids indicate that underplating of mantle-derived magmas may probably play a heat role in crustal melting. Assuming the mantle-derived melt has $\varepsilon_{Hf}(t) = 12$ and $\delta^{18}O = 5.3‰$ (King et al., 1998; Valley et al., 1998), and the sedimentary source melt has $\varepsilon_{Hf}(t) = -12$ and $\delta^{18}O = 10‰$ (Kemp et al., 2007; Li et al., 2009b), our modeling results are illustrated in Fig. 11B. The Bozhushan granites have low $\varepsilon_{Hf}(t)$ values (−9.5 to −6.1) and relatively high $\delta^{18}O$ values (7.9–9.6‰), which are lower than those having a sedimentary source but higher than mantle-derived magma. The results show that their source region might be composed of variable amounts of mafic and sedimentary components. Thus, we conclude that the Bozhushan granitoids might be derived from high-temperature melting of the Proterozoic mafic and metasedimentary basements of the Cathaysia block.

A conventional view is that highly fractionated S-type granite or the granitoids of ilmenite series are most favorable for tin mineralization because their parental magmas can produce copious Sn-rich fluids (Heinrich, 1990; Stemprok, 1990; Taylor and Wall, 1993). However, numerous tin deposits have recently been found to be associated with A-type granitoids in Nigeria, Brazil, America, Sinkiang and the Nanling district, China (Bi et al., 1992; Costi et al., 2002; Haapala and Lukkari, 2005; Jiang et al., 2006; Konopelko et al., 2009; Moura et al., 2007). The eastern Nanling region hosts many important tungsten deposits whereas the western Nanling region hosts many important tungsten deposits (Hua et al., 2010; Mao et al., 2007). Increasing numbers of granite plutons with tin

Table 2
Sr–Nd isotopic compositions of the Bozhushan granitic intrusion (BZS) and granite-porphyry veins in Bainiuchang ore district (DMS).

Sample no.	$^{87}Rb/^{86}Sr$	$^{87}Sr/^{86}Sr$	±1σ	$^{147}Sm/^{144}Nd$	$^{143}Nd/^{144}Nd$	±1σ	$(^{87}Sr/^{86}Sr)_i$	$(^{143}Nd/^{144}Nd)_i$	εNd (t)	T_{DM2} (Ma)
DMS-1	3.1	0.76479	11	0.10102	0.51201	3	0.7251	0.51195	−11.2	1802
BZS-1	2.2	0.71535	5	0.09765	0.51197	2	0.7127	0.51191	−12.0	1862
BZS-2	2.2	0.71535	18	0.10250	0.51199	2	0.7126	0.51193	−11.6	1833
BZS-3	2.1	0.72835	6	0.10938	0.51201	1	0.7257	0.51195	−11.3	1810
BZS-4	2.0	0.71557	6	0.10088	0.51198	2	0.7131	0.51192	−11.8	1848
BZS-5	2.2	0.71756	5	0.10232	0.51198	1	0.7148	0.51193	−11.7	1841
BZS-6	4.3	0.72200	6	0.10937	0.51197	2	0.7166	0.51191	−12.0	1866

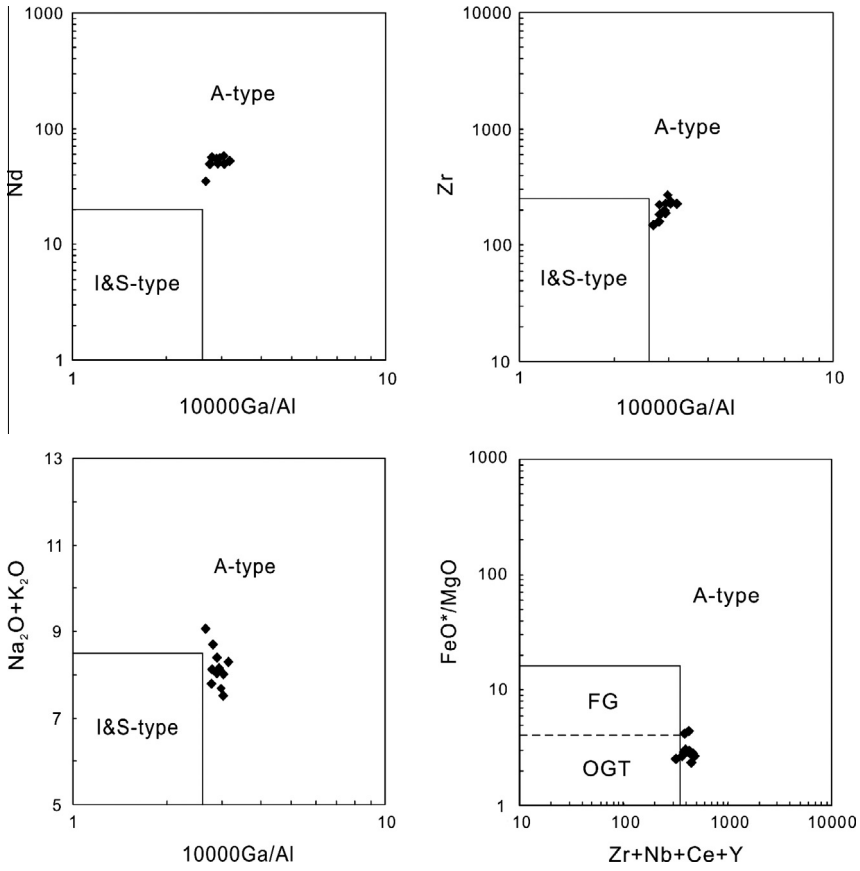

Fig. 10. K_2O vs. Na_2O diagram, Zr, Nb, Y, $K_2O + Na_2O$ vs. 10,000× Ga/Al diagram, and FeO/MgO vs. Zr + Nb + Ce + Y diagram of Whalen et al. (1987) for the Bozhushan granitic intrusion and granite porphyry veins in the Bainiuchang ore district.

mineralization have been classified as A-type granite plutons. These include the Qitianling pluton which hosts the Furong and Huaxiangling tin deposits, the Qianlishan pluton which hosts the Dongpo tin deposit, the Jiuyishan–Jinjiling pluton which hosts the Daao tin deposit, and the Huashan–Guposhan pluton which hosts the Xinlu tin deposit (Fu et al., 2005; Jiang et al., 2008, 2006; Wang et al., 2005; Zhao et al., 2012; Zhu et al., 2008). Mantle-derived materials appear to have played a larger role in the tin-bearing granite plutons than the tungsten-bearing granite plutons (Hua et al., 2010, 2007). In the western part of the Cathaysia bock which contains the Nanling region, Late Cretaceous mafic, ultramafic and alkaline rocks formed by mantle-derived magmas are widespread (Cheng and Mao, 2012; Liu et al., 2010a; Yan et al., 2005).

6.3. Implications for tectonic setting and mineralization

Previous age data show that the Bozhushan granite pluton was emplaced in Early-Cretaceous to Late-Eocene (Zhang and Chen, 1997; Cheng et al., 2010). Our new zircon U–Pb ages show that the pluton formed in a short period of time (85–88 Ma) in Late-Cretaceous. The cassiterite U–Pb age of the Bainiuchang silver-polymetallic deposits in the region determined by Li et al. (2013) using LA-ICP-MS is 87 ± 3 Ma is similar to the zircon U–Pb ages of the Bozhushan granite pluton. This establishes a clear temporal link between the Bozhushan granitoids and the silver-polymetallic mineralization in the region.

Late-Cretaceous granitoids (75–100 Ma, mostly 80–95 Ma) are widespread in the western part of the Cathaysia block including western Guangxi, southwest Guizhou and southeast Yunan (Cai et al., 2006; Cheng and Mao, 2010; Cheng et al., 2010, 2013b; Feng et al., 2013; Liang et al., 2011; Liu et al., 2007b). Important tin–tungsten deposits are associated with these granitoids (Deng et al., 2004; Li et al., 2013; Liu et al., 2007b; Mao et al., 2008a, 2007; Zhang et al., 2006; Zhao et al., 2007). Late-Cretaceous gabbro, diorite, alkaline rocks and lamprophyres are also common in the region (Cheng and Mao, 2012; Liu et al., 2010a; Yan et al., 2005). The occurrence of the bimodal magmatic suites supports the interpretation that the region was under the condition of lithospheric extension in the Late-Cretaceous (Cheng et al., 2013b; Liu et al., 2010a; Mao et al., 2008c; Suo et al., 1999; Yan et al., 2005). This indicates that the magmatism and related mineralization within western Cathaysia were associated to intraplate lithospheric extension. In fact, all Late Cretaceous granitoids in western Cathaysia are very similar in geochronology and tectonic background to the Bozhushan granites.

Recent research reveals that the Paleo-Pacific Plate changed subduction direction during the Late Cretaceous, resulting in large-scale continental lithospheric extension accompanied by significant volcanism, granite magmatism, and the formation of granite-related tin–tungsten mineralization in western Cathaysia. The WNW subduction of the Paleo-Pacific plate began in the Late-Jurassic (~160 Ma). The polarity of the subduction was switched to be sub-parallel to the eastern margin of the Eurasian after 135 Ma (Goldfarb et al., 2007; Maruyama et al., 1997; Niu et al., 2003). It is suggested that the change from lithospheric transpression to extension in South China at ~135 Ma is related to the change in plate motion at this time (Goldfarb et al., 2007; Mao et al., 2011, 2008b, 2007, 2006; Nie et al., 2004). Mao et al. (2008a) further suggested that the change in plate motion also induced delamination of the subducting slab and asthenospheric

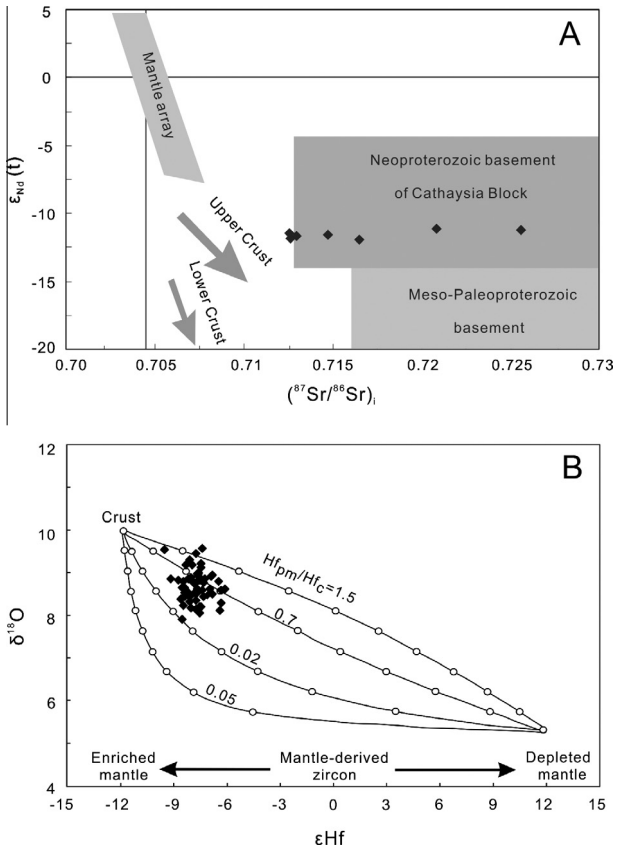

Fig. 11. (A) Diagram of Nd and Sr isotopic variation in the Bozhushan granitic intrusion and granite porphyry veins in the Bainiuchang ore district. Basement data are cited from Shen et al. (1995); and (B) diagram of $\varepsilon_{Hf}(t)$ vs. $\delta^{18}O$ variation in the Bozhushan granitic intrusion and granite porphyry veins in the Bainiuchang ore district (after Li et al., 2009b). Hf_{pm}/Hf_c is the ratio of Hf concentration in the parental mantle magma (pm) over crustal (c) melt indicated for each curves, and the small open circles on the curves represent 10% mixing increments by assuming the mantle zircon has $\varepsilon_{Hf}(t) = 12$ and $\delta^{18}O = 5.6‰$; the supercrustal zircon has $\varepsilon_{Hf}(t) = -12$ and $\delta^{18}O = 10‰$.

upwelling, which in turn cause mantle partial melting and melting of the lower and/or upper crust due to underplating of the mantle-derived magma. This could account for the presence of a range of igneous rocks in this region, with I-type, S-type, and A-type granites forming during the same magmatic event. The Late-Cretaceous granitoids and associated tin-polymetallic deposits in the Bainiuchang–Bozhushan area are thought to be the products of such tectono-magmatic event.

7. Conclusions

On the basis of zircon U–Pb geochronology and whole-rock geochemistry and isotopic compositions, the following conclusions can be reached.

(1) LA-MC-ICP-MS zircon U–Pb dating gives the crystallization ages of 85.97 ± 0.20–87.37 ± 0.32 Ma for the Bozhushan granite pluton which is located in southeastern Yunnan, southwest China. The Bozhushan granitoids belong to the A_2-subtype granite based on whole-rock chemical compositions.
(2) Whole-rock Sr–Nd isotopic data show that the parental magmas of the Bozhushan granitoids formed partial melting of the Proterozoic metasedimentary basement in the Cathaysia Block. The Hf–O isotopic compositions of zircon crystals from the granitoids indicate a dominant crustal source with minor contribution from the mantle for the parental magmas of the Bozhushan granitoids.
(3) The Bozhushan granite pluton is part of the Late-Cretaceous bimodal intrusive suites in the western part of the Cathaysia block stretching from southeastern Yunnan to western Guangxi. It is deduced that the granitoids and associated tin-polymetallic deposits formed in an intraplate setting under the conditions of lithospheric extension. Partial melting of the continental crust is believed to be related to asthenospheric upwelling.

Table A1
Zircon U–Pb LAICPMS analysis results of the Bozhushan granitic intrusion (BZS-1 and BZS-5) and granite-porphyry veins in Bainiuchang ore district (DMS).

Spot no.	Concentration (ppm)			Atomic ratios					Ages (Ma)	
	U	Th	Pb	$^{207}Pb/^{206}Pb$	$^{207}Pb/^{235}U$	1σ	$^{206}Pb/^{238}U$	1σ	$^{207}Pb/^{235}U$	$^{206}Pb/^{238}U$
BZS-1 (103°21′17″E, 23°21′55″N)										
1	1576	708	24.2	0.0479	0.0886	0.001614	0.0134	0.000093	86.2	86.0
2	656	266	10.3	0.0480	0.0886	0.002406	0.0135	0.000133	86.2	86.3
3	1599	606	24.2	0.0480	0.0891	0.001483	0.0134	0.000083	86.6	86.0
4	981	186	13.5	0.0481	0.0894	0.001936	0.0135	0.000106	86.9	86.2
5	1160	444	17.5	0.0489	0.0903	0.001722	0.0134	0.000102	87.8	85.6
6	1403	811	40.2	0.0499	0.0924	0.004249	0.0135	0.000177	89.7	86.4
7	1409	772	39.5	0.0485	0.0908	0.003570	0.0136	0.000154	88.3	87.0
8	1468	384	28.0	0.0491	0.0920	0.003904	0.0135	0.000186	89.3	86.3
9	2063	670	44.4	0.0462	0.0872	0.003577	0.0135	0.000198	84.9	86.6
10	1939	720	45.0	0.0450	0.0843	0.003751	0.0135	0.000193	82.2	86.4
11	1860	1214	57.3	0.0466	0.0884	0.003099	0.0136	0.000153	86.0	86.8
12	1486	461	31.6	0.0462	0.0865	0.003510	0.0135	0.000171	84.2	86.7
13	2052	1027	51.9	0.0461	0.0870	0.003003	0.0135	0.000138	84.7	86.5
14	1104	367	24.6	0.0458	0.0863	0.003736	0.0135	0.000173	84.0	86.8
15	1485	454	30.8	0.0441	0.0838	0.003540	0.0135	0.000179	81.7	86.6
16	1589	684	24.7	0.0515	0.0956	0.001802	0.0134	0.000098	92.7	86.1
17	1245	412	18.1	0.0510	0.0957	0.004655	0.0135	0.000105	92.8	86.4
18	1209	386	18.5	0.0514	0.0962	0.001777	0.0135	0.000093	93.3	86.4
19	1267	664	34.7	0.0519	0.0965	0.003778	0.0136	0.000167	93.5	86.8
BZS-5 (103°21′49″E, 23°21′58″N)										
1	1572	750	42.9	0.0476	0.0903	0.003472	0.0136	0.000155	87.8	87.4
2	1112	604	30.0	0.0502	0.0952	0.004602	0.0136	0.000192	92.3	86.9

(*continued on next page*)

Table A1 (*continued*)

Spot no.	Concentration (ppm)			Atomic ratios					Ages (Ma)	
	U	Th	Pb	$^{207}Pb/^{206}Pb$	$^{207}Pb/^{235}U$	1σ	$^{206}Pb/^{238}U$	1σ	$^{207}Pb/^{235}U$	$^{206}Pb/^{238}U$
3	1255	524	32.0	0.0452	0.0863	0.003356	0.0137	0.000145	84.1	87.9
4	1635	406	33.5	0.0444	0.0871	0.003459	0.0137	0.000182	82.9	87.8
5	1353	559	20.7	0.0474	0.0898	0.001648	0.0137	0.000103	87.4	87.8
6	1163	406	17.4	0.0477	0.0899	0.002105	0.0136	0.000101	87.5	86.8
7	1451	590	22.1	0.0457	0.0863	0.001731	0.0136	0.000096	84.1	87.1
8	971	1166	20.5	0.0528	0.0906	0.002313	0.0136	0.000111	97.3	87.4
9	2295	2346	43.9	0.0476	0.0900	0.001965	0.0136	0.000106	87.5	87.3
10	1470	485	21.8	0.0480	0.0910	0.001962	0.0136	0.000098	88.5	87.0
11	1473	351	20.9	0.0483	0.0920	0.001617	0.0137	0.000098	89.3	87.8
12	1660	1272	28.6	0.0502	0.0944	0.001609	0.0136	0.000083	91.6	86.9
13	1294	674	20.3	0.0478	0.0906	0.001966	0.0136	0.000089	88.0	87.3
14	1358	539	20.3	0.0485	0.0914	0.001538	0.0137	0.000097	88.8	87.7
15	1007	581	16.2	0.0522	0.0926	0.002684	0.0137	0.000102	95.5	87.5
16	1030	426	15.8	0.0477	0.0904	0.001845	0.0137	0.000106	87.9	87.9
17	1365	422	19.4	0.0485	0.0920	0.001603	0.0137	0.000095	89.4	87.4
DMS (Duimenshan ore block of Bainiuchang tin-polymetallic deposit)										
1	1645	565	24.3	0.0481	0.0888	0.001540	0.0134	0.000083	86.4	85.6
2	1227	343	17.8	0.0479	0.0887	0.001658	0.0134	0.000093	86.3	86.0
3	2139	910	32.5	0.0472	0.0878	0.001211	0.0134	0.000073	85.5	86.0
4	1442	391	21.2	0.0507	0.0941	0.001390	0.0135	0.000077	91.3	86.2
5	1205	541	18.6	0.0485	0.0903	0.001458	0.0135	0.000081	87.8	86.4
6	1283	475	19.3	0.0479	0.0890	0.001442	0.0134	0.000081	86.5	86.1
7	1423	474	21.3	0.0483	0.0904	0.001684	0.0135	0.000094	87.9	86.5
8	2173	675	31.8	0.0472	0.0869	0.001393	0.0133	0.000075	84.6	85.3
9	1576	454	23.1	0.0467	0.0867	0.001346	0.0134	0.000076	84.5	85.7
10	1595	478	23.5	0.0486	0.0904	0.001477	0.0135	0.000080	87.9	86.2
11	1378	439	20.8	0.0510	0.0951	0.001577	0.0134	0.000078	92.3	86.1
12	2185	841	32.9	0.0472	0.0874	0.001252	0.0134	0.000071	85.1	85.7
13	2845	1067	42.5	0.0476	0.0874	0.001115	0.0133	0.000076	85.1	85.2
14	2499	869	37.4	0.0476	0.0882	0.001165	0.0134	0.000077	85.8	85.9
15	1468	717	23.2	0.0485	0.0902	0.001371	0.0135	0.000083	87.7	86.1
16	1238	500	19.3	0.0499	0.0928	0.001750	0.0134	0.000093	90.1	86.1
17	1697	460	25.3	0.0494	0.0917	0.001467	0.0134	0.000095	89.1	86.1
18	1334	687	20.8	0.0466	0.0862	0.001395	0.0134	0.000083	84.0	85.8
19	1787	427	26.2	0.0484	0.0896	0.001575	0.0134	0.000075	87.1	85.8
20	1513	516	22.8	0.0483	0.0896	0.001452	0.0134	0.000077	87.2	86.0
21	1992	958	31.4	0.0481	0.0892	0.001260	0.0134	0.000079	86.8	86.0
22	919	275	13.5	0.0486	0.0894	0.001910	0.0134	0.000103	87.0	85.8
23	1825	616	27.4	0.0489	0.0902	0.001629	0.0134	0.000080	87.7	85.5
24	1417	685	36.3	0.0482	0.0902	0.003674	0.0135	0.000167	87.7	86.3
25	1290	476	29.5	0.0484	0.0911	0.004023	0.0135	0.000174	88.5	86.7
26	1518	289	28.0	0.0497	0.0933	0.003524	0.0136	0.000145	90.6	86.9
27	1399	453	31.3	0.0479	0.0901	0.003932	0.0136	0.000154	87.6	86.8
28	796	278	17.1	0.0471	0.0866	0.005085	0.0135	0.000187	84.4	86.4
29	1695	553	35.0	0.0503	0.0937	0.003954	0.0135	0.000178	90.9	86.3
30	1498	423	29.5	0.0482	0.0903	0.003631	0.0135	0.000177	87.8	86.7
31	1522	532	33.6	0.0483	0.0899	0.003605	0.0135	0.000165	87.5	86.7
32	1759	527	36.3	0.0490	0.0915	0.003446	0.0135	0.000150	88.9	86.4
33	1568	432	31.6	0.0487	0.0906	0.003702	0.0135	0.000160	88.1	86.3

Table A2
Hf and O isotopic compositions of zircons from the Bozhushan granitic intrusion (BZS-1 and BZS-5) and granite-porphyry veins in Bainiuchang ore district (DMS).

Spots	$T_{206/238}$ (Ma)	$^{176}Yb/^{177}Hf$	$\pm2\sigma$	$^{176}Lu/^{177}Hf$	$\pm2\sigma$	$^{176}Hf/^{177}Hf$	$\pm2\sigma$	$e_{Hf}(t)$	T_{DM2} (Ma)	$\delta^{18}O$	$\pm2\sigma$
BZS-1											
1	86	0.03	0.00017	0.0010	0.0000	0.282519	0.000016	−7.1	1605	8.48	0.35
2	86	0.02	0.00007	0.0008	0.0000	0.282495	0.000015	−8.0	1660	8.17	0.25
3	86	0.02	0.00010	0.0009	0.0000	0.282510	0.000013	−7.4	1625	8.21	0.27
4	86	0.03	0.00007	0.0009	0.0000	0.282486	0.000013	−8.3	1680	9.19	0.23
5	86	0.02	0.00018	0.0009	0.0000	0.282505	0.000015	−7.6	1637	8.98	0.35
6	86	0.03	0.00009	0.0009	0.0000	0.282513	0.000013	−7.3	1618	8.45	0.31
7	86	0.02	0.00104	0.0008	0.0000	0.282514	0.000016	−7.3	1617	8.77	0.39
8	86	0.04	0.00073	0.0013	0.0000	0.282541	0.000014	−6.3	1557	8.12	0.29
9	86	0.03	0.00011	0.0010	0.0000	0.282492	0.000013	−8.1	1666	8.44	0.36
10	86	0.03	0.00006	0.0010	0.0000	0.282480	0.000013	−8.5	1694	7.91	0.28
11	86	0.03	0.00026	0.0011	0.0000	0.282482	0.000013	−8.4	1689	8.23	0.40
12	86	0.03	0.00163	0.0009	0.0001	0.282548	0.000015	−6.1	1539	8.63	0.15
13	86	0.03	0.00045	0.0010	0.0000	0.282478	0.000015	−8.6	1698	8.40	0.35
14	86	0.03	0.00017	0.0011	0.0000	0.282542	0.000015	−6.3	1553	8.59	0.32
15	86	0.03	0.00083	0.0011	0.0000	0.282513	0.000013	−7.4	1620	9.58	0.41

Table A2 (*continued*)

Spots	$T_{206/238}$ (Ma)	$^{176}Yb/^{177}Hf$	±2σ	$^{176}Lu/^{177}Hf$	±2σ	$^{176}Hf/^{177}Hf$	±2σ	$e_{Hf}(t)$	T_{DM2} (Ma)	$\delta^{18}O$	±2σ
16	86	0.03	0.00021	0.0010	0.0000	0.282502	0.000013	−7.7	1643	8.15	0.24
17	86	0.03	0.00026	0.0012	0.0000	0.282507	0.000013	−7.5	1633	8.83	0.36
18	86	0.02	0.00008	0.0008	0.0000	0.282492	0.000014	−8.1	1666	8.33	0.38
19	86	0.03	0.00117	0.0010	0.0000	0.282542	0.000015	−6.3	1555	8.29	0.33
20	86	0.02	0.00009	0.0009	0.0000	0.282473	0.000011	−8.7	1708	8.83	0.37
BZS-5											
1	87	0.03	0.00002	0.0010	0.0000	0.282483	0.000015	−8.4	1687	8.79	0.29
2	87	0.03	0.00039	0.0011	0.0000	0.282509	0.000014	−7.5	1628	9.21	0.28
3	87	0.02	0.00020	0.0007	0.0000	0.282505	0.000014	−7.6	1636	9.01	0.37
4	87	0.03	0.00028	0.0012	0.0000	0.282492	0.000013	−8.1	1667	9.30	0.38
5	87	0.01	0.00036	0.0005	0.0000	0.282450	0.000013	−9.5	1757	9.54	0.40
6	87	0.02	0.00014	0.0009	0.0000	0.282502	0.000015	−7.7	1613	9.45	0.35
7	87	0.03	0.00018	0.0011	0.0000	0.282507	0.000014	−7.5	1642	8.84	0.33
8	87	0.02	0.00007	0.0009	0.0000	0.282480	0.000013	−8.5	1631	8.65	0.39
9	87	0.03	0.00043	0.0012	0.0000	0.282507	0.000014	−7.5	1693	8.07	0.25
10	87	0.02	0.00009	0.0009	0.0000	0.282524	0.000013	−6.9	1562	8.62	0.34
11	87	0.02	0.00051	0.0007	0.0000	0.282526	0.000014	−6.8	1633	8.91	0.37
12	87	0.02	0.00007	0.0007	0.0000	0.282509	0.000012	−7.5	1592	9.13	0.21
13	87	0.03	0.00083	0.0011	0.0000	0.282525	0.000013	−6.9	1589	8.92	0.28
14	87	0.03	0.00009	0.0010	0.0000	0.282494	0.000014	−8.0	1627	8.89	0.32
15	87	0.03	0.00023	0.0011	0.0000	0.282461	0.000013	−9.2	1592	8.85	0.46
16	87	0.03	0.00029	0.0012	0.0000	0.282528	0.000014	−6.8	1661	8.95	0.31
17	87	0.03	0.00016	0.0011	0.0000	0.282506	0.000015	−7.6	1735	8.97	0.49
18	87	0.03	0.00028	0.0010	0.0000	0.282490	0.000014	−8.1	1585	8.85	0.39
DMS											
1	86	0.03	0.00012	0.0010	0.0000	0.282497	0.000019	−7.9	1634	9.17	0.25
2	86	0.03	0.00048	0.0012	0.0000	0.282498	0.000018	−7.9	1670	8.77	0.34
3	86	0.03	0.00036	0.0010	0.0000	0.282509	0.000017	−7.5	1655	8.21	0.23
4	86	0.03	0.00033	0.0010	0.0000	0.282501	0.000015	−7.8	1654	8.75	0.36
5	86	0.03	0.00028	0.0011	0.0000	0.282509	0.000015	−7.5	1629	8.88	0.28
6	86	0.03	0.00013	0.0010	0.0000	0.282504	0.000016	−7.7	1647	8.61	0.29
7	86	0.03	0.00019	0.0011	0.0000	0.282484	0.000013	−8.4	1629	8.44	0.20
8	86	0.03	0.00042	0.0011	0.0000	0.282501	0.000015	−7.8	1640	8.52	0.39
9	86	0.03	0.00012	0.0009	0.0000	0.282491	0.000016	−8.1	1684	8.85	0.38
10	86	0.02	0.00009	0.0008	0.0000	0.282483	0.000015	−8.4	1646	8.66	0.32
11	86	0.03	0.00043	0.0010	0.0000	0.282490	0.000014	−8.1	1668	8.55	0.30
12	86	0.02	0.00022	0.0009	0.0000	0.282503	0.000016	−7.7	1685	8.55	0.35
13	86	0.03	0.00013	0.0011	0.0000	0.282492	0.000017	−8.1	1670	8.44	0.41
14	86	0.02	0.00018	0.0008	0.0000	0.282503	0.000014	−7.7	1641	8.36	0.38
15	86	0.03	0.00036	0.0012	0.0000	0.282484	0.000017	−8.4	1666	8.55	0.31
16	86	0.02	0.00057	0.0007	0.0000	0.282511	0.000015	−7.4	1641	8.59	0.36
17	86	0.04	0.00109	0.0015	0.0000	0.282530	0.000014	−6.8	1685	8.51	0.25
18	86	0.02	0.00055	0.0007	0.0000	0.282538	0.000016	−6.4	1623	8.81	0.29
19	86	0.02	0.00026	0.0007	0.0000	0.282515	0.000015	−7.2	1613	8.85	0.36

Acknowledgments

This work was jointly supported by the Key Project of National Natural Science Foundation of China (41230316)" and the "National Basic Research Program of China (973 Program, 2014CB440906)". We would like to thank Prof. Chu-Si Li for sharing ideas during this study.

Appendix A

See Tables A1 and A2.

References

Anderson, J.L., 1983. Proterozoic anorogenic granite plutonism of North America. Geol. Soc. Am. Mem. 161, 133–154.
Bi, C.S., Sheng, X.Y., Xu, Q.S., 1992. New discovery of tin deposit related with Hercynian A-type granite in China. Sci. China Ser. B – Chem, 632–638.
Bonin, B., 2007. A-type granites and related rocks: evolution of a concept, problems and prospects. Lithos 97, 1–29.
Cai, M.H., He, L.Q., Liu, G.Q., Wu, D.C., Huang, H.M., 2006. SHRIMP zircon U–Pb dating of the intrusive rocks in the Dachang tin-polymetallic ore field, Guangxi and their geological significance. Geol. Rev. 52, 409–414.
Chappell, B.W., White, A.J.R., 1992. I- and S-type granites in the Lachlan fold belt. R. Soc. Edinburgh Trans. 83, 1–26.
Chappell, B.W., Wyborn, D., 2012. Origin of enclaves in S-type granites of the Lachlan fold belt. Lithos 154, 235–247.
Chappell, B.W., White, A.J.R., Wyborn, D., 1987. The importance of residual source material (restite) in granite petrogenesis. J. Petrol. 28, 1111–1138.
Chen, X.M., Lin, Z., Xie, F.C., 1998. Geological and geochemical characteristics of the Bainiuchang super-large silver polymentallic deposit of superimposed mineralization, Yunnan Province. Sci. Geol. Sin. 33, 115.
Chen, X.M., Deng, J., Bai, J.G., Shen, C.H., 2000. Ore-forming fluid system of the Paleozoic sedimentary basin in Bainiuchang ore district, Yunnan province. Sci. Geol. Sin. 14, 171–173.
Cheng, Y.B., Mao, J.W., 2010. Age and geochemistry of granites in Gejiu area, Yunnan province, SW China: constraints on their petrogenesis and tectonic setting. Lithos 120, 258–276.
Cheng, Y.B., Mao, J.W., 2012. Geochronology of the gabbro-mafic microgranular enclaves-granite associations in the Gejiu district, Yunnan Province and their geodynamic significance. Acta Geol. Sin. – Engl. Ed. 86, 748–761.
Cheng, Y.B., Mao, J.W., Chen, X.L., Li, W., 2010. LA-ICP-MS zircon U–Pb dating of the Bozhushan granite in southeastern Yunnan province and its significance. J. Jilin Univ. Earth Sci. Ed. 40, 869–878.
Cheng, Y.B., Mao, J.W., Chang, Z.S., Pirajno, F., 2013a. The origin of the world class tin-polymetallic deposits in the Gejiu district, SW China: constraints from metal zoning characteristics and 40Ar/39Ar geochronology. Ore Geol. Rev. 53, 50–62.
Cheng, Y.B., Mao, J.w., Spandler, C., 2013b. Petrogenesis and geodynamic implications of the Gejiu igneous complex in the western Cathaysia block, South China. Lithos 175, 213–229.
Clemens, J.D., 2003. S-type granitic magmas – petrogenetic issues, models and evidence. Earth Sci. Rev. 61, 1–18.
Clemens, J.D., 2006. Melting of continental crust: fluid regimes, melting reactions, and source-rock fertility. In: Brown, M., Rushmer, T. (Eds.), Evolution and Differentiation of Continental Crust. Cambridge University Press, New York, pp. 296–330.

Clemens, J.D., Holloway, J.R., White, A.J.R., 1986. Origin of an A-type granite: experimental constraints. Am. Mineral. 71, 317–324.
Collins, W.J., Beams, S.D., White, A.J.R., Chappell, B.W., 1982. Nature and origin of A-type granites with particular reference to southeastern Australia. Contrib. Miner. Petrol. 80, 189–200.
Costi, H.T., Dall'Agnol, R., Borges, R.M.K., Minuzzi, O.R.R., Teixeira, J.T., 2002. Tin-bearing sodic episyenites associated with the Proterozoic, A-type Agua Boa granite, Pitinga mine, Amazonian craton, Brazil. Gondwana Res. 5, 435–451.
Deng, J., Chen, X.M., Rao, Y.Q., Sun, Z.S., Cheng, X.J., Shen, C.H., Wang, Q.F., 2004. Two kinds of compaction fluid systems of the Nanling area and their mineralizations. Geoscience 18, 1–7.
Eby, G.N., 1990. The A-type granitoids: a review of their occurrence and chemical characteristics and speculations on their petrogenesis. Lithos 26, 115–134.
Feng, J.R., Mao, J.W., Pei, R.F., 2013. Ages and geochemistry of Laojunshan granites in southeastern Yunnan, China: implications for W–Sn polymetallic ore deposits. Mineral. Petrol. 107, 573–589.
Frost, C.D., Frost, B.R., 1997. Reduced rapakivi-type granites: the tholeiite connection. Geology 25, 647–650.
Fu, J.M., Ma, C.Q., Xie, C.F., Zhang, Y.M., Peng, S.B., 2005. Ascertainment of the Jinjiling aluminous A-type granite, Hunan Province and its tectonic settings. Geochimica 34, 215–226.
Goldfarb, R.J., Hart, C., Davis, G., Groves, D., 2007. East Asian gold: deciphering the anomaly of phanerozoic gold in precambrian cratons. Econ. Geol. 102, 341–345.
Goodge, J.W., Vervoort, J.D., 2006. Origin of mesoproterozoic A-type granites in laurentia: Hf isotope evidence. Earth Planet. Sci. Lett. 243, 711–731.
Gu, L.G., Liu, Y.P., Li, C.Y., Xu, W., Ye, L., 2009. SHRIMP zircon U–Pb geochronology and lithogeochemistry of Caledonian Granites from the Laojunshan area, southeastern Yunnan province, China: implications for the collision between the Yangtze and Cathaysia blocks. Geochem. J. 43, 101–122.
Haapala, I., Lukkari, S., 2005. Petrological and geochemical evolution of the Kymi stock, a topaz granite cupola within the Wiborg rapakivi batholith, Finland. Lithos 80, 347–362.
Haapala, I., Ramo, O.T., Frindt, S., 2005. Comparison of Proterozoic and Phanerozoic rift-related basaltic-granitic magmatism. Lithos 80, 1–32.
Heinrich, C.A., 1990. The chemistry of hydrothermal tin (-tungsten) ore deposition. Econ. Geol. 85, 457–481.
Hua, R.M., Zhang, W.L., Gu, S.Y., Chen, P.R., 2007. Comparison between REE granite and W–Sn granite in the Nanling region, South China, and their mineralizations. Acta Petrol. Sin. 23, 2321–2328.
Hua, R.M., Li, G.L., Zhang, W.L., Hu, D.Q., Chen, P.R., Chen, W.F., Wang, X.D., 2010. A tentative discussion on differences between large-scale tungsten and tin mineralizations in South China. Miner. Deposits 29, 9–23.
Ishihara, S., 2007. Origin of the Cenozoic–Mesozoic magnetite-series and ilmenite-series granitoids in East Asia. Gondwana Res. 11, 247–260.
Jahn, B.M., Wu, F.Y., Chen, B., 2000. Massive granitoid generation in Central Asia: Nd isotope evidence and implication for continental growth in the Phanerozoic. Episodes 23, 82–92.
Jiang, S.Y., Zhao, K.D., Jiang, Y.H., Ling, H.F., Ni, P., 2006. New type of tin mineralization related to granite in South China: evidence from mineral chemistry, element and isotope geochemistry. Acta Petrol. Sin. 22, 2509–2516.
Jiang, S., Zhao, K., Jiang, Y., Dai, B., 2008. Characteristics and genesis of Mesozoic A-type granites and associated mineral deposits in the Southern Hunan and Northern Guangxi provinces along the Shi-Hang belt, South China. Geol. J. China Univ. 14, 496–509.
Kemp, A.I.S., Hawkesworth, C.J., Foster, G.L., Paterson, B.A., Woodhead, J.D., Hergt, J.M., Gray, C.M., Whitehouse, M.J., 2007. Magmatic and crustal differentiation history of granitic rocks from Hf–O isotopes in zircon. Science 315, 980–983.
Kerr, A., Fryer, B.J., 1993. Nd isotope evidence for crust-mantle interaction in the generation of A-type granitoid suites in Labrador, Canada. Chem. Geol. 104, 39–60.
King, P.L., White, A.J.R., Chappell, B.W., Allen, C.M., 1997. Characterization and origin of aluminous A-type granites from the Lachlan fold belt, Southeastern Australia. J. Petrol. 38, 371–391.
King, E.M., Valley, J.W., Davis, D.W., Edwards, G.R., 1998. Oxygen isotope ratios of Archean plutonic zircons from granite–greenstone belts of the Superior Province. Indicator of magmatic source. Precambr. Res. 92, 365–387.
Konopelko, D., Seltmann, R., Biske, G., Lepekhina, E., Sergeev, S., 2009. Possible source dichotomy of contemporaneous post-collisional barren I-type vs. tin-bearing A-type granites, lying on opposite sides of the South Tien Shan suture. Ore Geol. Rev. 35, 206–216.
Li, Z.X., Li, X.H., Kinny, P.D., Wang, J., Zhang, S., Zhou, H., 2003. Geochronology of Neoproterozoic syn-rift magmatism in the Yangtze Craton, South China and correlations with other continents: evidence for a mantle superplume that broke up Rodinia. Precambr. Res. 122, 85–109.
Li, X.H., Li, W.X., Li, Z.X., Lo, C.H., Wang, J., Ye, M.F., Yang, Y.H., 2009a. Amalgamation between the Yangtze and Cathaysia Blocks in South China: constraints from SHRIMP U–Pb zircon ages, geochemistry and Nd–Hf isotopes of the Shuangxiwu volcanic rocks. Precambr. Res. 174, 117–128.
Li, X.H., Li, W.X., Wang, X.C., Li, Q.L., Liu, Y., Tang, G.Q., 2009b. Role of mantle-derived magma in genesis of early Yanshanian granites in the Nanling Range, South China: in situ zircon Hf–O isotopic constraints. Sci. China Ser. D – Earth Sci. 52, 1262–1278.
Li, Z.X., Li, X.H., Wartho, J.A., Clark, C., Li, W.X., Zhang, C.L., Bao, C.M., 2010. Magmatic and metamorphic events during the early Paleozoic Wuyi–Yunkai orogeny, southeastern South China: new age constraints and pressure-temperature conditions. Geol. Soc. Am. Bull. 122, 772–793.
Li, K.W., Geng, J.Z., Liu, H., Zhang, Q., Wang, D.P., Cai, Y., 2011. Polymetallic mineralization related with the late Yanshanian granitic magmatism in the southeastern Yunnan province. Acta Miner. Sin., 607–608
Li, K.W., Zhang, Q., Wang, D.P., Cai, Y., Liu, Y.P., 2013. LA-MC-ICP-MS U–Pb Geochronology of cassiterite from the Bainiuchang polymetallic deposit, Yunnan Province, China. Acta Miner. Sin. 33, 203–209.
Liang, T., Wang, D.H., Hou, K.J., Li, H.Q., Huang, H.M., Cai, M.H., Wang, D.M., 2011. LA-MC-ICP-MS zircon U–Pb dating of Longxianggai pluton in Dachang of Guangxi and its geological significance. Acta Petrol. Sin. 27, 1624–1636.
Litvinovsky, B.A., Jahn, B.M., Zanvilevich, A.N., Saunders, A., Poulain, S., Kuzmin, D.V., Reichow, M.K., Titov, A.V., 2002. Petrogenesis of syenite-granite suites from the Bryansky Complex (Transbaikalia, Russia): implications for the origin of A-type granitoid magmas. Chem. Geol. 189, 105–133.
Liu, J.S., Zhang, H.P., Ouyang, Y.F., Zhang, C.H., 2007a. Bainiuchang super-large silver-polymetallic ore deposit related to granitic magmatism in Mengzi, Yunnan. J. Cent. South Univ. Technol. 14, 568–574.
Liu, Y.P., Li, Z.X., Li, H.M., Guo, L.G., Xu, W., Ye, L., Li, C.Y., Pi, D.H., 2007b. U–Pb geochronology of cassiterite and zircon from the Dulong Sn–Zn deposit: evidence for Cretaceous large-scale granitic magmatism and mineralization events in southeastern Yunnan province, China. Acta Petrol. Sin. 23, 967–976.
Liu, S., Su, W.C., Hu, R.Z., Feng, C.X., Gao, S., Coulson, I.M., Wang, T., Feng, G.Y., Tao, Y., Xia, Y., 2010a. Geochronological and geochemical constraints on the petrogenesis of alkaline ultramafic dykes from southwest Guizhou Province, SW China. Lithos 114, 253–264.
Liu, Y.S., Hu, Z.C., Zong, K.Q., Gao, C.G., Gao, S., Xu, J.A., Chen, H.H., 2010b. Reappraisement and refinement of zircon U–Pb isotope and trace element analyses by LA-ICP-MS. Chin. Sci. Bull. 55, 1535–1546.
Loiselle, M.C., Wones, D.R., 1979. Characteristics and origin of anorogenic granites, vol. 11(468). Abstracts of papers to be presented at the Annual Meetings of the Geological Society of America and Associated Societies, San Diego, California, November 5–8.
Luo, J.L., 1995. The metallogenic characteristics of super-large deposits in Yunnan Province. Yunnan Geol. 14, 276–280.
Mao, J.W., Xie, G.Q., Li, X.F., Zhang, C.Q., Wang, Y.T., 2006. Mesozoic large-scale mineralization and multiple lithospheric extensions in South China. Acta Geol. Sin. – Engl. Ed. 80, 420–431.
Mao, J.W., Xie, G.Q., Guo, C.L., Chen, Y.C., 2007. Large-scale tungsten–tin mineralization in the Nanling region, South China: metallogenic ages and corresponding geodynamic processes. Acta Petrol. Sin. 23, 2329–2338.
Mao, J.W., Cheng, Y.B., Guo, C.L., Yang, Z.X., Feng, J.R., 2008a. Gejiu tin polymetallic ore-field: deposit model and discussion for several points concerned. Acta Geol. Sinica 82, 1455–1467.
Mao, J.W., Xie, G.Q., Bierlein, F., Que, W.J., Du, A.D., Ye, H.S., Pirajno, F., Li, H.M., Guo, B.J., Li, Y.F., Yang, Z.Q., 2008b. Tectonic implications from Re-Os dating of Mesozoic molybdenum deposits in the East Qinling-Dabie orogenic belt. Geochim. Cosmochim. Acta 72, 4607–4626.
Mao, J.W., Xie, G.Q., Guo, C.L., Yuan, S.D., Cheng, Y.B., Chen, Y.C., 2008c. Spatial-Temporal distribution of Mesozoic ore deposits in South China and their metallogenic settings. Geol. J. China Univ. 14, 510–526.
Mao, J.W., Pirajno, F., Xiang, J.F., Gao, J.J., Ye, H.S., Li, Y.F., Guo, B.J., 2011. Mesozoic molybdenum deposits in the east Qinling-Dabie orogenic belt: characteristics and tectonic settings. Ore Geol. Rev. 43, 264–293.
Mao, J.W., Cheng, Y.B., Chen, M.H., Pirajno, F., 2013. Major types and time-space distribution of Mesozoic ore deposits in South China and their geodynamic settings. Miner. Deposita 48, 267–294.
Maruyama, S., Isozaki, Y., Kimura, G., Terabayashi, M., 1997. Paleogeographic maps of the Japanese Islands: plate tectonic synthesis from 750 Ma to the present. Island Arc 6, 121–142.
Middlemost, E.A.K., 1994. Naming materials in the magma/igneous rock system. Earth Sci. Rev. 37, 215–224.
Moura, M.A., Botelho, N.F., de Mendonca, F.C., 2007. The indium-rich sulfides and rare arsenates of the Sn–In-mineralized mangabeira A-type granite, central Brazil. Can. Mineral. 45, 485–496.
Nie, F.J., Jiang, S.H., Liu, Y., 2004. Intrusion-related gold deposits of North China craton, People's Republic of China. Resour. Geol. 54, 299–324.
Niu, B.G., He, Z.J., Song, B., Lin, J.S., 2003. SHRIMP dating of the Zhangjiakou volcanic series and its significance. Geol. Bull. China 22, 140–141.
Patiño Douce, A.E., 1997. Generation of metaluminous A-type granites by low-pressure melting of calc-alkaline granitoids. Geology 25, 743–746.
Pei, R.F., Wang, Y.L., Wang, H.L., 2009. Ore-forming specialty of the tectono-magmatic zone in Nanling region and its emplacement dynamics for metallogenic series of W–Sn polymetallic deposits. Geol. China 36, 483–489.
Qi, L., Hu, J., Gregoire, D.C., 2000. Determination of trace elements in granites by inductively coupled plasma mass spectrometry. Talanta 51, 507–513.
Rickwood, P.C., 1989. Boundary lines within petrologic diagrams which use oxides of major and minor elements. Lithos 22, 247–263.
Rudnick, R.L., Fountain, D.M., 1995. Nature and composition of the continental crust: a lower crustal perspective. Rev. Geophys. 33, 267–309.
Shen, W.Z., Wang, D.Z., Liu, C.S., 1995. Isotope geochemical characteristics and material sources of tin-bearing porphyries in South China. Acta Geol. Sinica 69, 349–359.
Skjerlie, K.P., Johnston, A.D., 1993. Vapor-absent melting at 10 kbar of a biotite- and amphibole-bearing tonalitic gneiss: implications for the generation of A-type granites. Geology 21, 89–90.
Stemprok, M., 1990. Solubility of tin, tungsten and molybdenum oxides in felsic magmas. Miner. Deposita 25, 205–212.

Sun, S.S., McDonou gh, W.F., 1989. Chemical and isotopic systematics of oceanic basalt: implications for mantle composition and processes. Geol. Soc. Spec. Publ. 42, 528–548.
Sun, W.D., Yang, X.Y., Fan, W.M., Wu, F.Y., 2012. Mesozoic large scale magmatism and mineralization in South China. Lithos 150, 1–5.
Suo, S.T., Bi, X.H., Zhou, H.W., 1999. Very Low Grade Metamorphism. Geological Publishing House, pp. 1–68.
Taylor, J.R., Wall, V.J., 1993. Cassiterite solubility, tin speciation, and transport in a magmatic aqueous phase. Econ. Geol. Bull. Soc. Econ. Geol. 88, 437–460.
Turner, S.P., Foden, J.D., Morrison, R.S., 1992. Derivation of some A-type magmas by fractionation of basaltic magma: an example from the Padthaway Ridge, South Australia. Lithos 28, 151–179.
Valley, J.W., Chiarenelli, J.R., McLelland, J.M., 1994. Oxygen isotope geochemistry of zircon. Earth Planet. Sci. Lett. 126, 187–206.
Valley, J.W., Kinny, P.D., Schulze, D.J., Spicuzza, M.J., 1998. Zircon megacrysts from kimberlites: oxygen Isotope variability among mantle melts. Contrib. Miner. Petrol. 133, 1–11.
Valley, J.W., Lackey, J.S., Cavosie, A.J., Clechenko, C.C., Spicuzza, M.J., Basei, M.A.S., Bindeman, I.N., Ferreira, V.P., Sial, A.N., King, E.M., Peck, W.H., Sinha, A.K., Wei, C.S., 2005. 4.4 billion years of crustal maturation: oxygen isotope ratios of magmatic zircon. Contrib. Miner. Petrol. 150, 561–580.
Wang, Q., Zhao, Z.H., Jian, P., Xiong, X.L., Bao, Z.W., Dai, T.M., Xu, J.F., Ma, J.L., 2005. Geochronology of Cretaceous, A-type granitoids or alkaline intrusive rocks in the hinterland, South China: constraints for late-Mesozoic tectonic evolution. Acta Petrol. Sin. 21, 795–808.
Wang, Q., Wyman, D.A., Li, Z.X., Bao, Z.W., Zhao, Z.H., Wang, Y.H., Jian, P., Yang, Y.H., Chen, L.L., 2010. Petrology, geochronology and geochemistry of ca. 780 Ma A-type granites in South China: petrogenesis and implications for crustal growth during the breakup of the supercontinent Rodinia. Precambr. Res. 178, 185–208.
Watson, E.B., Harrison, T.M., 1983. Zircon saturation revisited: temperature and composition effects in a variety of crustal magma types. Earth Planet. Sci. Lett. 64, 295–304.
Whalen, J.B., Currie, K.L., Chappell, B.W., 1987. A-type granites: geochemical characteristics, discrimination and petrogensis. Contrib. Miner. Petrol. 95, 407–419.
Wu, F.Y., Jahn, B.M., Wilde, S., Sun, D.Y., 2000. Phanerozoic crustal growth: U–Pb and Sr–Nd isotopic evidence from the granites in northeastern China. Tectonophysics 328, 89–113.
Wu, F.Y., Sun, D.Y., Li, H.M., Jahn, B.M., Wilde, S., 2002. A-type granites in northeastern China: age and geochemical constraints on their petrogenesis. Chem. Geol. 187, 143–173.
Wu, F.Y., Yang, Y.H., Xie, L.W., Yang, J.H., Xu, P., 2006. Hf isotopic compositions of the standard zircons and baddeleyites used in U–Pb geochronology. Chem. Geol. 234, 105–126.
Wu, F.Y., Li, X.H., Zheng, Y.F., Gao, S., 2007. Lu-Hf isotopic systematics and their applications in petrology. Acta Petrol. Sin. 23, 185–220.
Yan, D.P., Zhou, M.F., Wang, Y., Wang, C.L., Zhao, T.P., 2005. Structural styles and chronological evidences from Dulong-Song Chay tectonic dome: earlier spreading of South China Sea Basin due to Late Mesozoic to Early Cenozoic extension of South China Block. Earth Sci. 30, 402–412.
Yang, J.H., Wu, F.Y., Chung, S.L., Wilde, S.A., Chu, M.F., 2006. A hybrid origin for the Qianshan A-type granite, northeast China: geochemical and Sr–Nd–Hf isotopic evidence. Lithos 89, 89–106.
Zhang, S.T., Chen, C.G., 1997. Geological characteristics and evolution rule of Bozhushan complex granite in southeastern Yunnan. Yunnan Geol. 16, 222–232.
Zhang, H.P., Liu, J.S., Li, X.B., Zhang, X.L., 2006. Relationship of granites to tin, silver, copper, lead, zinc, polymetallic deposits in southeastern Yunnan, China. Contrib. Geol. Miner. Resour. Res. 21, 87–90.
Zhang, Q., Li, K.W., Wang, D.P., Hou, X.F., 2009. New geological and geochemical evidence of Bainiuchang polymetallic deposit in southeastern Yunnan. Acta Miner. Sin., 355–356
Zhang, Q., Wang, D.P., Li, K.W., Cai, Y., 2011. The genesis of super-large cassiterite-sulfide deposits in the western of Nanling – hydrothermal sedimentation or magma hydrothermalism? Acta Miner. Sin., 132–133
Zhao, K.D., Jiang, S.Y., Ni, P., Ling, H.F., Jiang, Y.H., 2007. Sulfur, lead and helium isotopic compositions of sulfide minerals from the Dachang Sn-polymetallic ore district in South China: implication for ore genesis. Mineral. Petrol. 89, 251–273.
Zhao, K.D., Jiang, S.Y., Yang, S.Y., Dai, B.Z., Lu, J.J., 2012. Mineral chemistry, trace elements and Sr–Nd–Hf isotope geochemistry and petrogenesis of Cailing and Furong granites and mafic enclaves from the Qitianling batholith in the Shi-Hang zone, South China. Gondwana Res. 22, 310–324.
Zhou, J.P., Xu, K.Q., Hua, R.M., 1998. Characteristics and genesis of exhalative sedimentary massive sulfides in southeastern Yunnan Province. Acta Miner. Sin. 18, 158–168.
Zhu, J.C., Chen, J., Wang, R.C., Lu, J.J., Xie, L., 2008. Early Yanshanian NE trending Sn/W-bearing A-type granites in the western-middle part of the Nanling Mts region. Geol. J. China Univ. 14, 474–484.
Zhu, C.H., Liu, S.X., Zhang, Q., Gu, D.M., 2010. The exhalative-sedimentary evidence of the Bainiuchang Ag-polymetallic deposit, Yunnan, China: constraints from geochemistry of host-rocks. Geoscience 24, 120–130.